

Sample-Optimal Quantum State Tomography for Structured Quantum States in One Dimension

Zhen Qin, Casey Jameson, Alireza Goldar, Michael B. Wakin, Zhexuan Gong and Zhihui Zhu*

Abstract

While quantum state tomography (QST) remains the gold standard for benchmarking and verifying quantum devices, it requires an exponentially large number of measurements and classical computational resources for generic quantum many-body systems, making it impractical even for intermediate sized quantum devices. Fortunately, many physical quantum states often exhibit certain low-dimensional structures that enable the development of efficient QST. A notable example is the class of states represented by matrix product operators (MPOs) with a finite matrix/bond dimension, which include most physical states in one dimension and where the number of independent parameters describing the states only grows *linearly* with the number of qubits n . A recent study [1] has proved that, with Haar random projective measurements, only a $O(n^3)$ number of state copies is required to guarantee bounded recovery error of such an MPO state. While this result provides a formal evidence that quantum states with an efficient classical representation can be reconstructed with an efficient number of state copies, the number of state copies required is still significantly larger than the number of independent parameters in the classical representation.

In this paper, we attempt to narrow this gap and study whether the number of state copies can saturate the information theoretic bound (i.e., $O(n)$, the number of parameters in the MPOs) using physical quantum measurements. We answer this question affirmatively by using a class of Informationally Complete Positive Operator-Valued Measures (IC-POVMs), including symmetric IC-POVMs (SIC-POVMs) and spherical t -designs. For SIC-POVMs and (approximate) spherical 2-designs, we show that the number of state copies to guarantee bounded recovery error of an MPO state with a constrained least-squares estimator depends on the probability distribution of the MPO under the POVM but scales only linearly with n when the distribution is approximately uniform. For spherical t -designs with $t \geq 3$, we prove that only a number of state copies proportional to the number of independent parameters in the MPO is needed for a guaranteed recovery of any state represented by an MPO. Moreover, we propose a projected gradient descent (PGD) algorithm to solve the constrained least-squares problem and show that it can efficiently find an estimate with bounded recovery error when appropriately initialized.

We emphasize that our results focus on the sample complexity and have not taken into account the complexity in implementing the required measurement settings. In practice, the SIC-POVM or the spherical t -designs with $t \geq 2$ has no known efficient implementation using local quantum circuits. We provide numerical evidence that local SIC-POVMs, which can be implemented efficiently and readily on current quantum hardware, can be used to perform QST for certain MPO states with a $O(n)$ number of state copies using the proposed PGD algorithm.

1 Introduction

The state of a quantum system composed of n qudits (which are d -level quantum systems; qubits have $d = 2$) is fully described by a density matrix $\rho \in \mathbb{C}^{d^n \times d^n}$ with unit trace and is positive semidefinite (PSD) [2]. To reconstruct or estimate the density matrix, quantum measurements need to be performed on numerous identical copies of the state. Any such physical measurement is characterized by a Positive Operator-Valued Measure (POVM), which can be represented by a set of PSD matrices $\{\mathbf{A}_1, \dots, \mathbf{A}_K\}$ that collectively sum to the identity matrix, i.e., $\sum_{k=1}^K \mathbf{A}_k = \mathbf{I}_{d^n}$. Each matrix \mathbf{A}_k ($k = 1, \dots, K$) in the POVM corresponds to a potential measurement outcome, and the probability of obtaining that outcome is given by $p_k = \text{trace}(\mathbf{A}_k \rho)$. The probabilistic nature of quantum measurements necessitates multiple measurements (say M) with the same POVM to obtain statistically accurate estimates $\hat{p}_k = \frac{f_k}{M}$ of each p_k ,

*ZQ (email: qin.660@osu.edu) and ZZ (email: zhu.3440@osu.edu) are with the Department of Computer Science and Engineering, the Ohio State University; CJ (email: cwjameson@mines.edu) and ZG (email: gong@mines.edu) are with the Department of Physics, Colorado School of Mines; and AG (email: goldar@mines.edu) and MBW (email: mwakin@mines.edu) are with the Department of Electrical Engineering, Colorado School of Mines.

where f_k denotes the number of times the k -th outcome is observed in the M experiments. Disregarding statistical errors, $\{p_k\}$ can be considered as K linear measurements of the state ρ . From a machine learning perspective, we can refer to $\{p_k\}$ and their empirical estimates $\{\hat{p}_k\}$ as population and empirical measurements of the state, respectively. The goal of quantum state tomography (QST) [3] is to find the density matrix from empirical measurements with high accuracy. As the density matrix provides full information about the quantum state, QST remains the gold standard for benchmarking and verifying quantum devices.

Extensive research efforts, both in algorithmic development [4–15] and theoretical analysis [16–21], have been devoted to QST. For generic quantum states, the required state copies must grow exponentially with the number of qubits. This sampling complexity can be improved for low-rank density matrices [18,20], but it still grows exponentially with n . To implement QST effectively on current quantum computers with over 100 qubits [22–24], it is important to exploit more compact structures within practical states of interest. A notable example is the class of states represented by matrix product operators (MPOs)¹. The density matrix elements of such states can be expressed as the following matrix product [25,26]

$$\rho(i_1 \cdots i_n, j_1 \cdots j_n) = \mathbf{X}_1^{i_1, j_1} \mathbf{X}_2^{i_2, j_2} \cdots \mathbf{X}_n^{i_n, j_n}, \quad (1)$$

where i_k ($k = 1, 2, \dots, n$) labels a basis of the k -th qubit, and $\mathbf{X}_\ell^{i_\ell, j_\ell} \in \mathbb{C}^{r_{\ell-1} \times r_\ell}$ with $r_0 = r_n = 1$. The dimensions $\mathbf{r} = (r_1, \dots, r_{n-1})$ are often called the *bond dimensions*² of the MPO in quantum physics, though we may also call them the *MPO ranks*. An MPO comprises nd^2 matrices, each with a dimension of at most $\bar{r} \times \bar{r}$ where the matrix dimension $\bar{r} = \max_\ell r_\ell$ determines the efficiency of the representation. Thus, an MPO can be efficiently represented with $O(nd^2\bar{r}^2)$ number of parameters. The decomposition (1) is also mathematically equivalent to the tensor train (TT) decomposition used for compact representation of large tensors [27].

Examples of states that can be represented by MPOs include ground states of most quantum systems in one dimension [28], general Hamiltonians with decaying long-range interactions [29], and those generated by noisy quantum computers, where the noise could also limit the amount of quantum entanglement and thus enable an efficient state representation [26]. Several approaches, such as maximum likelihood estimation [30,31] and tensor train cross approximation [32], have empirically demonstrated the scalable number of state copies when employing MPO in QST. Nevertheless, the theoretical analysis of this advantage has remained ambiguous in previous studies. Recently, we successfully obtained a theoretical guarantee on the recovery error of an MPO state using multiple Haar random projective measurements [1]. To be specific, for any given $\epsilon > 0$, we prove that with $\Omega(nd^2\bar{r}^2 \log n)$ different sets of Haar random projective measurement bases and $\Omega(n^3 d^2 \bar{r}^2 \log n / \epsilon^2)$ total number of state copies, a properly constrained least-squares minimization using the empirical measurements stably recovers the ground-truth state with ϵ -closeness in the Frobenius norm with high probability. While this result formally shows that MPOs can be reconstructed using an efficient number of state copies, it is not sample optimal as the scaling n^3 is much larger than the degrees of freedom ($O(n)$) in the MPOs. In addition, this work [1] provides a projected gradient descent (i.e., iterative hard threshold) algorithm for performing the QST in practice, but does not provide a formal guarantee for that algorithm.

1.1 Main contributions

Our work aims to address two fundamental questions regarding the QST of states represented by MPOs:

1. *Is there a measurement setting that can provably recover an MPO with a number of state copies proportional to the number of parameters in the MPO?*
2. *If so, can we develop a provably correct algorithm to reconstruct MPOs from the obtained measurements?*

We provide positive answers to both the above questions by utilizing informationally complete POVMs (IC-POVM). An IC-POVM is defined by the property that every quantum state is uniquely determined by its measurement statistics. Beyond QST, IC-POVMs with special ties find applications in quantum cryptography [33], quantum fingerprinting [34], and are relevant to foundational studies of quantum mechanics [35,36]. It eliminates the inherent randomness in Haar random POVMs that are often used to establish optimal sample complexity [20]. Without this inherent randomness, we can more easily analyze the effects of statistical errors in the recovery error bound and the design provable optimization algorithms.

¹MPOs representing physical quantum states are also termed matrix product density operators (MPDO).

²It is also common to simply call $\bar{r} = \max\{r_1, \dots, r_{n-1}\}$ the bond dimension.

We begin by studying recovery guarantees for MPOs from empirical quantum measurements (physical measurements containing statistical errors) obtained using a class of IC-PVOMs including the rank-one symmetric IC-POVM (SIC-POVM) [37] and more broadly spherical t -design POVMs that are induced by (approximate) spherical t -designs [38,39]. *The first contribution of this paper—presented in Section 3—is a new sampling complexity bound (refers to the number of state copies) that matches the number of parameters in MPOs to guarantee bounded recovery error for a particular estimator—the solution to a constrained least-squares optimization problem.* Specifically, for SIC-POVM and 2-design POVMs, our result shows that $M = \Omega(nd^2\gamma(\rho)\bar{r}^2 \log n/\epsilon^2)$ number of state copies is sufficient to achieve ϵ -accuracy in recovering the ground-truth state ρ in the Frobenius norm, where $\gamma(\rho) = K \cdot \max_{k=1}^K p_k$ captures the uniformity of the probabilistic distribution of the measurement. The term $\gamma(\rho)$ can be as small as 1, but in some cases, it may be as large as d^n ; however, for many cases it is only polynomially large in n . The dependence of $\gamma(\rho)$ could be eliminated by using spherical t -designs with $t \geq 3$, for which our sampling complexity bound is improved to $M = \Omega(nd^2\bar{r}^2 \log n/\epsilon^2)$. Excluding the logarithmic term, this bound exhibits linear dependence on n , d^2 , and \bar{r}^2 , aligning precisely with the degrees of freedom $O(nd^2\bar{r}^2)$ in MPOs and is thus sample optimal. This result improves upon previous work [1] using Haar random projective measurement bases that require $\Omega(nd^2\bar{r}^2 \log n)$ POVMs and $\Omega(n^3 d^2 \bar{r}^2 \log n/\epsilon^2)$ total number of state copies. We summarize the main results and comparison with our previous result [1] in Table 1.

Table 1: Comparison with existing work for estimating n -qudits MPOs (with bond dimension \bar{r}) to achieve ϵ -closeness in the Frobenius norm. The result for SIC/2-designs depends on $\gamma(\rho) = K \cdot \max_k p_k$, i.e., the probability distribution of measuring the state ρ with the corresponding POVM.

POVM	# POVMs	# total state copies
Haar random ([1, Theorem 5])	$\Omega(nd^2\bar{r}^2 \log n)$	$\Omega(\frac{n^3 d^2 \bar{r}^2 \log n}{\epsilon^2})$
SIC/2-designs (Theorem 1)	1	$\Omega(\frac{nd^2\gamma(\rho)\bar{r}^2 \log n}{\epsilon^2})$
t -designs, $t \geq 3$ (Theorem 2)	1	$\Omega(\frac{nd^2\bar{r}^2 \log n}{\epsilon^2})$

The second contribution of this paper—presented in Section 4—is the development of a projected gradient descent (PGD) with guaranteed convergence analysis for solving the abovementioned constrained least-squares optimization problem. In each iteration, the algorithm performs gradient update, followed by a projection back to the MPO format with a unit trace. Even without the constraint on the trace, computing the optimal projection onto the set of MPOs is challenging and could be NP-hard [40]. We employ a sequential approach called TT-SVD [27]—developed for computing TT decomposition which is equivalent to MPO—for computing an approximate projection. While TT-SVD is not optimal, it is computationally efficient and comes with a sub-optimal guarantee. Leveraging this guarantee, we show that, with an appropriate initialization, PGD converges linearly to a vicinity of the ground-truth state, with a distance matching the results in Table 1. In addition, we show that spectral initialization provides a valid starting point, ensuring the convergence of PGD. Our numerical experiments in Section 5 suggest that PGD can also efficiently find the underlying state even with a random initialization.

1.2 Notation

We use calligraphic letters (e.g., \mathcal{X}) to denote tensors, bold capital letters (e.g., \mathbf{X}) to denote matrices, bold lowercase letters (e.g., \mathbf{x}) to denote column vectors, and italic letters (e.g., x) to denote scalar quantities. Elements of matrices and tensors are denoted in parentheses. For example, $\mathcal{X}(i_1, i_2, i_3)$ denotes the element in position (i_1, i_2, i_3) of the order-3 tensor \mathcal{X} . The calligraphic letter \mathcal{A} is reserved for the linear measurement map. For a positive integer K , $[K]$ denotes the set $\{1, \dots, K\}$. The superscripts $(\cdot)^\top$ and $(\cdot)^\dagger$ denote the transpose and Hermitian transpose, respectively³. For two matrices \mathbf{A}, \mathbf{B} of the same size, $\langle \mathbf{A}, \mathbf{B} \rangle = \text{trace}(\mathbf{A}^\dagger \mathbf{B})$ denotes the inner product between them. $\|\mathbf{X}\|$ and

³As is conventional in the quantum physics literature (but not in information theory and signal processing), we use $(\cdot)^\dagger$ to denote the Hermitian transpose.

$\|\mathbf{X}\|_F$ respectively represent the spectral norm and Frobenius norm of \mathbf{X} . $\sigma_i(\mathbf{X})$ is the i -th singular value of \mathbf{X} . For a vector \mathbf{a} of size $N \times 1$, its l_n -norm is defined as $\|\mathbf{a}\|_n = (\sum_{m=1}^N |a_m|^n)^{\frac{1}{n}}$. For two positive quantities $a, b \in \mathbb{R}$, the inequality $b \lesssim a$ or $b = O(a)$ means $b \leq ca$ for some universal constant c ; likewise, $b \gtrsim a$ or $b = \Omega(a)$ represents $b \geq ca$ for some universal constant c . To simplify notations in the following sections, for an order- n TT format with ranks (r_1, \dots, r_n) , we define $\bar{r} = \max_{i=1}^{n-1} r_i$.

2 Informationally Complete POVM

As described in the introduction, the population measurements $\{p_k\}$ of the density matrix ρ from a POVM $\{\mathbf{A}_k\}$ are linear measurements that can be described through a linear map $\mathcal{A} : \mathbb{C}^{d^n \times d^n} \rightarrow \mathbb{R}^K$ of the form

$$\mathcal{A}(\rho) = \begin{bmatrix} \langle \mathbf{A}_1, \rho \rangle \\ \vdots \\ \langle \mathbf{A}_K, \rho \rangle \end{bmatrix}. \quad (2)$$

If a POVM consists of at least d^{2n} matrices such that we can form exactly d^{2n} linearly independent matrices by linear combination, it is said to be an informationally complete POVM (IC-POVM) [41–43]. IC-POVMs consisting of exactly d^{2n} elements are called minimal [44]. In this section, we introduce some common IC-POVMs, including symmetric IC-POVM and spherical t -designs, and present properties of the corresponding linear mappings \mathcal{A} .

Symmetric Informationally Complete POVM (SIC-POVM) A particularly attractive and potentially useful IC-POVM is one that is *symmetric*, i.e., it has equal pairwise inner products between any pair of the POVM elements [37, 45]. A POVM that is informationally complete, minimal, and symmetric is called SIC-POVM.

Definition 1. ([46]) *A Symmetric Informationally Complete POVM (SIC-POVM) consists of d^{2n} rank-one POVM elements $\{\mathbf{A}_k\}$ that satisfies (i) each with an equivalent trace $\text{trace}(\mathbf{A}_k) = \frac{1}{d^n}$ for all $k \in [d^{2n}]$, and (ii) every pair*

of measurement operators satisfies $\langle \mathbf{A}_k, \mathbf{A}_j \rangle = \begin{cases} \frac{1}{d^{2n}}, & k = j, \\ \frac{1}{d^{2n}(d^n+1)}, & k \neq j. \end{cases}$

The set of vectors comprising an SIC-POVM has been extensively studied in various contexts under different names [37], such as equiangular lines in linear algebra [47] and equalangular tight frames in information theory [48]. In quantum information, it has also found extensive applications, including quantum state tomography [49] and quantum cryptography [50]. SIC-POVMs have been numerically constructed for matrix dimensions ranging from 2 to 151 [51, 52], and for many higher dimensions, up to 39,604 [53]. While it is widely believed that SIC-POVMs exist in all dimensions, no explicit construction of the SIC-POVM is known for an arbitrary dimension of the Hilbert space. The following result establishes stable embeddings of any Hermitian matrices from SIC-POVM in terms of $\|\mathcal{A}(\rho)\|_2^2$.

Lemma 1. *Suppose that $\{\mathbf{A}_k\}_{k=1}^{d^{2n}}$ form an SIC-POVM. Then for any Hermitian matrix $\rho \in \mathbb{C}^{d^n \times d^n}$, $\mathcal{A}(\rho)$ satisfies*

$$\|\mathcal{A}(\rho)\|_2^2 = \sum_{k=1}^{d^{2n}} \langle \mathbf{A}_k, \rho \rangle^2 = \frac{\|\rho\|_F^2 + (\text{trace}(\rho))^2}{d^n(d^n+1)}. \quad (3)$$

The proof is provided in Appendix A. By using tools from compressive sensing literature [54–58], the previous work [1] provides a similar stable embedding result from Haar random projective measurement bases, but only for MPOs. In contrast, with POVM being informationally complete, (3) holds for any Hermitian matrices without relying on any randomness in the measurement operator. This allows us to develop tight sampling complexity bound in Section 3 and iterative algorithms with guaranteed convergence in Section 4. As an immediate consequence of Lemma 1, for any two density matrices ρ_1 and ρ_2 , the difference $\rho_1 - \rho_2$ remains Hermitian, and hence

$$\|\mathcal{A}(\rho_1 - \rho_2)\|_2^2 = \frac{\|\rho_1 - \rho_2\|_F^2 + (\text{trace}(\rho_1 - \rho_2))^2}{d^n(d^n+1)} = \frac{\|\rho_1 - \rho_2\|_F^2}{d^n(d^n+1)}, \quad (4)$$

where we use the property that $\text{trace}(\rho_1) = \text{trace}(\rho_2) = 1$. Thus, SIC-POVM not only ensures distance measurements ($\mathcal{A}(\rho_1) \neq \mathcal{A}(\rho_2)$) as long as $\rho_1 \neq \rho_2$, but also exactly preserves the distance of the two states in the measurement space, up to a universal scaling $1/d^n(d^n+1)$.

t -design POVMs A more general set of IC-POVM are those induced by spherical t -designs.

Definition 2. (Spherical t -designs [16,59]). A finite set $\{\mathbf{w}_k\}_{k=1}^K \subset \mathbb{C}^{d^n}$ of normalized vectors is called a spherical quantum t -design if⁴

$$\frac{1}{K} \sum_{k=1}^K (\mathbf{w}_k \mathbf{w}_k^\dagger)^{\otimes s} = \int (\mathbf{w} \mathbf{w}^\dagger)^{\otimes s} d\mathbf{w} \quad (5)$$

holds for any $s \leq t$, where the integral on the right hand side is taken with respect to the Haar measure on the complex unit sphere in \mathbb{C}^{d^n} .

When $s = 1$, we have $\frac{1}{K} \sum_{k=1}^K \mathbf{w}_k \mathbf{w}_k^\dagger = \int \mathbf{w} \mathbf{w}^\dagger d\mathbf{w} = \frac{1}{d^n} \mathbf{I}$, and hence $\mathbf{A}_k = \frac{d^n}{K} \mathbf{w}_k \mathbf{w}_k^\dagger, k = 1, \dots, K$ form a rank-one POVM. For simplicity, we call such an induced POVM $\{\mathbf{A}_k = \frac{d^n}{K} \mathbf{w}_k \mathbf{w}_k^\dagger\}$ as a t -design POVM. SIC-POVM is a special instance of 2-design POVMs. In (5), we adopt the setting of uniform weights ($1/K$ for each \mathbf{w}_k , which is mostly commonly used in practice) to simplify the analysis, but one can consider a more general scenario of varied weights [39]. Unlike SIC-POVM, t -designs always exist and can, in principle, be constructed in any dimension and for any t [61,62], although in some cases these constructions can be inefficient, as they require vector sets of exponential size [63]. Instead, we may use approximate t -designs which can be efficiently implemented in practice [64].

Definition 3. (Spherical δ -approximate t -designs [64]). A finite set $\{\mathbf{w}_k\}_{k=1}^K \subset \mathbb{C}^{d^n}$ of normalized vectors is called a spherical quantum δ -approximate t -design if

$$(1 - \delta) \int (\mathbf{w} \mathbf{w}^\dagger)^{\otimes s} d\mathbf{w} \leq \frac{1}{K} \sum_{k=1}^K (\mathbf{w}_k \mathbf{w}_k^\dagger)^{\otimes s} \leq (1 + \delta) \int (\mathbf{w} \mathbf{w}^\dagger)^{\otimes s} d\mathbf{w} \quad (6)$$

holds for any $s \geq 2$, where the integral on the right hand side is taken with respect to the Haar measure on the complex projective space. In addition, $\frac{1}{K} \sum_{k=1}^K \mathbf{w}_k \mathbf{w}_k^\dagger = \frac{1}{d^n} \mathbf{I}$.

The following result generalizes Lemma 1 to t -design POVMs and approximate t -design POVMs.

Lemma 2. Suppose that $\{\mathbf{w}_k\}_{k=1}^K \subset \mathbb{C}^{d^n}$ forms an δ -approximate t -design ($t \geq 2$). Let \mathcal{A} be the linear map in (2) corresponding to the induced POVM $\{\mathbf{A}_k = \frac{d^n}{K} \mathbf{w}_k \mathbf{w}_k^\dagger\}$. Then for arbitrary Hermitian matrix $\rho \in \mathbb{C}^{d^n \times d^n}$, $\mathcal{A}(\rho)$ satisfies

$$(1 - \delta) \frac{d^n (\|\rho\|_F^2 + (\text{trace}(\rho))^2)}{K(d^n + 1)} \leq \|\mathcal{A}(\rho)\|_2^2 \leq (1 + \delta) \frac{d^n (\|\rho\|_F^2 + (\text{trace}(\rho))^2)}{K(d^n + 1)}. \quad (7)$$

The proof is given in Appendix B. Similar to (4), it follows from Lemma 2 that for any two density matrices ρ_1 and ρ_2 , $\mathcal{A}(\rho_1 - \rho_2)$ satisfies

$$\|\mathcal{A}(\rho_1 - \rho_2)\|_2^2 \geq (1 - \delta) \frac{d^n (\|\rho_1 - \rho_2\|_F^2 + (\text{trace}(\rho_1 - \rho_2))^2)}{K(d^n + 1)} = (1 - \delta) \frac{d^n \|\rho_1 - \rho_2\|_F^2}{K(d^n + 1)}. \quad (8)$$

3 Stable Recovery of Matrix Product Operators

Building upon the results that a (approximate) t -design POVM $\{\mathbf{A}_1, \dots, \mathbf{A}_K\} \in \mathbb{C}^{d^n \times d^n}$ provides unique population measurements for any state, in this section, we investigate the stable recovery for MPOs of form (1) from empirical measurements acquired through such POVMs. Specifically, for an MPO $\rho^* \in \mathbb{C}^{d^n \times d^n}$ with ranks (r_1, \dots, r_{n-1}) , we use the POVM to measure it M times and take the average of the outcomes to generate empirical probabilities

$$\hat{p}_k = \frac{f_k}{M}, \quad k = 1, \dots, K, \quad (9)$$

where f_k denotes the number of times the k -th output is observed. We denote $\hat{\mathbf{p}} = [\hat{p}_1 \ \dots \ \hat{p}_K]^\top$ as the empirical measurements obtained by the POVM, which are unbiased estimators of the population measurements $\mathbf{p} =$

⁴ $K \geq C_{d^n + \lceil t/2 \rceil - 1}^{\lceil t/2 \rceil} \cdot C_{d^n + \lceil t/2 \rceil - 1}^{\lceil t/2 \rceil}$ is necessary to form a spherical t -design[49,60].

$[p_1 \cdots p_K]^\top = \mathcal{A}(\rho^*)$, where \mathcal{A} is the induced linear measurement operator formally defined in (2). To simplify the notation for the analysis, we denote by $\boldsymbol{\eta} = [\eta_1, \dots, \eta_K]^\top = \widehat{\boldsymbol{p}} - \boldsymbol{p}$ the statistical error between the empirical probabilities and population probabilities.

With empirical measurements $\widehat{\boldsymbol{p}}$, we consider minimizing the following constrained least squares objective:

$$\widehat{\boldsymbol{\rho}} = \arg \min_{\boldsymbol{\rho} \in \mathbb{X}_r} \|\mathcal{A}(\boldsymbol{\rho}) - \widehat{\boldsymbol{p}}\|_2^2, \quad (10)$$

where we denote by \mathbb{X}_r the set of MPOs with ranks $\boldsymbol{r} = (r_1, \dots, r_{n-1})$:

$$\mathbb{X}_r = \left\{ \boldsymbol{\rho} \in \mathbb{C}^{d^n \times d^n} : \boldsymbol{\rho} = \boldsymbol{\rho}^\dagger, \text{trace}(\boldsymbol{\rho}) = 1, \boldsymbol{\rho}(i_1 \cdots i_n, j_1 \cdots j_n) = \mathbf{X}_1^{i_1, j_1} \mathbf{X}_2^{i_2, j_2} \cdots \mathbf{X}_n^{i_n, j_n}, \right. \\ \left. \mathbf{X}_\ell^{i_\ell, j_\ell} \in \mathbb{C}^{r_{\ell-1} \times r_\ell}, \ell = 1, \dots, n-1, r_0 = r_n = 1 \right\}. \quad (11)$$

It is worth noting that one could consider imposing additional structure on the factors $\mathbf{X}_\ell^{i_\ell, j_\ell}$ to ensure that $\boldsymbol{\rho}$ is PSD, as done in [65, eq. (3)]. However, the condition in [65, eq. (3)] is only sufficient, not necessary, for ensuring $\boldsymbol{\rho}$ is PSD and adding PSD constraint does not significantly reduce the number of degrees of freedom of elements in the set \mathbb{X}_r . Hence, we focus on the set (11), which encompasses not only PSD matrices but also non-PSD matrices.

Assuming a global solution for (10) can be found, our objective is to study the performance of $\widehat{\boldsymbol{\rho}}$, and examine how the recovery error $\|\widehat{\boldsymbol{\rho}} - \rho^*\|_F$ scales with the size of the MPO (specifically in relation to the number of qudits n) and the number of measurements M . In order to achieve a stable estimation of the state with a polynomial number of measurements relative to n , we expect the recovery error exhibits polynomial growth rather than exponential growth with respect to n . Next section will provide iterative algorithm to solve (10).

Main results We now provide a formal analysis of the recovery error $\|\widehat{\boldsymbol{\rho}} - \rho^*\|_F$. Since both SIC-POVM and exact t -design POVM can be viewed as specific instances of δ -approximate t -design POVMs, the analysis will primarily focus on δ -approximate t -design POVM. Using the fact that $\widehat{\boldsymbol{\rho}}$ is a global solution of (10) and the fact that $\rho^* \in \mathbb{X}_r$, we have

$$\begin{aligned} 0 &\leq \|\mathcal{A}(\rho^*) - \widehat{\boldsymbol{p}}\|_2^2 - \|\mathcal{A}(\widehat{\boldsymbol{\rho}}) - \widehat{\boldsymbol{p}}\|_2^2 \\ &= \|\mathcal{A}(\rho^*) - \mathcal{A}(\rho^*) - \boldsymbol{\eta}\|_2^2 - \|\mathcal{A}(\widehat{\boldsymbol{\rho}}) - \mathcal{A}(\rho^*) - \boldsymbol{\eta}\|_2^2 \\ &= 2\langle \mathcal{A}(\rho^*) + \boldsymbol{\eta}, \mathcal{A}(\widehat{\boldsymbol{\rho}} - \rho^*) \rangle + \|\mathcal{A}(\rho^*)\|_2^2 - \|\mathcal{A}(\widehat{\boldsymbol{\rho}})\|_2^2 \\ &= 2\langle \boldsymbol{\eta}, \mathcal{A}(\widehat{\boldsymbol{\rho}} - \rho^*) \rangle - \|\mathcal{A}(\widehat{\boldsymbol{\rho}} - \rho^*)\|_2^2, \end{aligned} \quad (12)$$

which further implies that

$$\|\mathcal{A}(\widehat{\boldsymbol{\rho}} - \rho^*)\|_2^2 \leq 2\langle \boldsymbol{\eta}, \mathcal{A}(\widehat{\boldsymbol{\rho}} - \rho^*) \rangle. \quad (13)$$

According to (8) for δ -approximate t -design POVM, the left-hand side of the above equation can be further lower bounded by

$$\|\mathcal{A}(\widehat{\boldsymbol{\rho}} - \rho^*)\|_2^2 \geq (1 - \delta) \frac{d^n \|\widehat{\boldsymbol{\rho}} - \rho^*\|_F^2}{K(d^n + 1)}. \quad (14)$$

The challenge part is to deal with the right-hand side of (13). A straightforward application of the Cauchy–Schwarz inequality $\langle \boldsymbol{\eta}, \mathcal{A}(\widehat{\boldsymbol{\rho}} - \rho^*) \rangle \leq \|\boldsymbol{\eta}\|_2 \cdot \|\mathcal{A}(\widehat{\boldsymbol{\rho}} - \rho^*)\|_2$ is insufficient for providing a tight result as $\|\boldsymbol{\eta}\|_2$ scales as $\frac{1}{\sqrt{M}}$ according to [1, eq. (35)]. Instead, we leverage the randomness of $\boldsymbol{\eta}$ and employ the following concentration bound for multinomial random variables.

Lemma 3. ([1, Lemma 3]) *Suppose (f_1, \dots, f_K) are mutually independent and follow the multinomial distribution Multinomial(M, \boldsymbol{p}) where $\sum_{k=1}^K f_i = M$ and $\boldsymbol{p} = [p_1, \dots, p_K]$. Let a_1, \dots, a_K be fixed. Then, for any $t > 0$,*

$$\mathbb{P} \left(\sum_{k=1}^K a_k \left(\frac{f_k}{M} - p_k \right) > t \right) \leq e^{-\frac{Mt}{4a_{\max}}} \min \left\{ 1, \frac{a_{\max} t}{4 \sum_{k=1}^K a_k^2 p_k} \right\} + e^{-\frac{Mt^2}{8 \sum_{k=1}^K a_k^2 p_k}}, \quad (15)$$

where $a_{\max} = \max_k |a_k|$.

We proceed by considering the following two cases, 2-designs and t -designs with $t \geq 3$.

Case (i): 2-designs. There are two potential technical difficulties in directly applying Lemma 3 to bound the term $\langle \boldsymbol{\eta}, \mathcal{A}(\widehat{\boldsymbol{\rho}} - \boldsymbol{\rho}^*) \rangle$ by plugging in $a_k = \langle \mathbf{A}_k, \widehat{\boldsymbol{\rho}} - \boldsymbol{\rho}^* \rangle$: (1) a_k is not independent to the random variables $\{f_k\}$ since $\widehat{\boldsymbol{\rho}}$ depends on the empirical measurements, and (2) we need to upper bound a term of form $\sum_{k=1}^K \langle \mathbf{A}_k, \boldsymbol{\rho} - \boldsymbol{\rho}^* \rangle^2 p_k$ originating from the exponential term in (15). We will address the first challenge by using a covering argument. For the second challenge, to utilize the upper bound for $\|\mathcal{A}(\boldsymbol{\rho} - \boldsymbol{\rho}^*)\|_2^2 = \sum_{k=1}^K \langle \mathbf{A}_k, \boldsymbol{\rho} - \boldsymbol{\rho}^* \rangle^2$ in Section 2, we capture the largest probabilities by

$$\gamma(\boldsymbol{\rho}^*) := K \cdot \max_k p_k = K \cdot \max_k \langle \mathbf{A}_k, \boldsymbol{\rho}^* \rangle. \quad (16)$$

Since $\max_k p_k \geq \frac{1}{K}$, $\gamma(\boldsymbol{\rho}^*) \geq 1$ always holds. When the probability distribution is uniform, $\gamma(\boldsymbol{\rho}^*)$ can be small as $O(1)$; particularly, $\gamma(\boldsymbol{\rho}^*) = 1$ when $p_1 = \dots = p_K = 1/K$. On the other hand, if the probability distribution is spiky, $\gamma(\boldsymbol{\rho}^*)$ could approach K . We now summarize the main result as follows.

Theorem 1 (Stable recovery with 2-designs). *Suppose $\{\mathbf{A}_1, \dots, \mathbf{A}_K\}$ form a set of δ -approximate 2-design POVMs. Consider an MPO state $\boldsymbol{\rho}^* \in \mathbb{C}^{d^n \times d^n}$ with ranks (r_1, \dots, r_{n-1}) . Then, with the empirical measurements $\widehat{\boldsymbol{\rho}}$ obtained by measuring the state M times using the POVM and probability $1 - e^{-\Omega(nd^2\bar{r}^2 \log n)}$, the solution $\widehat{\boldsymbol{\rho}}$ of the constrained least squares (10) satisfies*

$$\|\widehat{\boldsymbol{\rho}} - \boldsymbol{\rho}^*\|_F \lesssim \frac{d\bar{r} \sqrt{(1+\delta)n\gamma(\boldsymbol{\rho}^*) \log n}}{(1-\delta)\sqrt{M}}. \quad (17)$$

The proof is given in Appendix C. Theorem 1 guarantees a stable recovery of the ground-truth state with a δ -approximate 2-design POVM when the number of state copies $M \geq \Omega(nd^2\gamma(\boldsymbol{\rho}^*)\bar{r}^2 \log n/\epsilon^2)$. This condition highlights that the growth of M is only polynomial in terms of the number of qudits n when $\gamma(\boldsymbol{\rho}^*)$ is small. In particular, when $\gamma(\boldsymbol{\rho}^*) = O(1)$, we can achieve an optimal theoretical bound for M that matches $O(nd^2\bar{r}^2)$, the number of degrees of freedom of MPOs. On the other hand, when $\gamma(\boldsymbol{\rho}^*)$ is polynomial in terms of n , the order of M still remains polynomial.

As mentioned above, $\gamma(\boldsymbol{\rho}) \geq 1$ always holds. To further illustrate possible values for $\gamma(\boldsymbol{\rho})$, we consider the case of SIC-POVM. First consider an identity density matrix $\boldsymbol{\rho} = \frac{1}{d^n} \mathbf{I}_{d^n} = \frac{1}{d} \mathbf{I}_d \otimes \dots \otimes \frac{1}{d} \mathbf{I}_d$ which can be written as an MPO with bond dimension 1. For this case, $\langle \mathbf{A}_k, \boldsymbol{\rho} \rangle = \frac{1}{d^n} \text{trace}(\mathbf{A}_k) = \frac{1}{d^{2n}}$ for all k , and hence $\gamma(\boldsymbol{\rho}) = 1$. On the other hand, when $\boldsymbol{\rho} = d^n \mathbf{A}_k$ for some k (note that such a rank-one density matrix may not be an MPO), we have $\langle \mathbf{A}_k, \boldsymbol{\rho} \rangle = \frac{1}{d^n}$ and $\langle \mathbf{A}_j, \boldsymbol{\rho} \rangle = \frac{1}{d^n(d^n+1)}$ for all $j \neq k$, and hence $\gamma(\boldsymbol{\rho}) = d^n$. Indeed, we can prove that $\gamma(\boldsymbol{\rho}) \leq d^n$ always holds for any state $\boldsymbol{\rho}$ since $\langle \mathbf{A}_k, \boldsymbol{\rho} \rangle \leq \|\boldsymbol{\rho}\| \text{trace}(\mathbf{A}_k) \leq \text{trace}(\mathbf{A}_k) = \frac{1}{d^n}$ for all k . However, we note that the above pathological case with spiky probability distribution may happen rarely in practice. For instance, consider a random density matrix $\boldsymbol{\rho} = \mathbf{u}\mathbf{u}^\dagger$, where⁵ each entry in $\mathbf{u} \in \mathbb{C}^{d^n}$ is generated i.i.d. from a complex normal distribution $\mathcal{CN}(0, \frac{1}{d^n})$. In this case, each term $\langle \mathbf{A}_k, \mathbf{u}\mathbf{u}^\dagger \rangle$ has mean $\mathbb{E}[\langle \mathbf{A}_k, \mathbf{u}\mathbf{u}^\dagger \rangle] = \frac{\text{trace}(\mathbf{A}_k)}{d^n} = \frac{1}{d^{2n}}$. Moreover, since $\langle \mathbf{A}_k, \mathbf{u}\mathbf{u}^\dagger \rangle$ is a second-order polynomial in the entries of Gaussian random vector, it is a subexponential random variable [66, Proposition 2.4] with subexponential norm⁶ $\|\langle \mathbf{A}_k, \mathbf{u}\mathbf{u}^\dagger \rangle - \frac{1}{d^{2n}}\|_{\psi_1} \leq \frac{c}{d^n} \|\sqrt{d^n} \mathbf{u}\|_{\psi_2}^2 \|\mathbf{A}_k\|_F + \frac{1}{d^{2n}} \lesssim \frac{1}{d^{2n}}$ for some constant c . We can then invoke concentration inequality for subexponential random variable [67] to obtain that $\max_k \langle \mathbf{A}_k, \boldsymbol{\rho} \rangle \lesssim \frac{n}{d^{2n}}$ holds with probability at least $1 - e^{-Cn}$ for some positive constant C . In other words, for such a random density matrix $\boldsymbol{\rho}$, with high probability the probability distribution under SIC-POVM is quite uniform as $\gamma(\boldsymbol{\rho}) \lesssim n$.

Finally, we note that the dependence of $\gamma(\boldsymbol{\rho}^*)$ may arise from technical difficulties, and could be eliminated by more sophisticated analysis, which is left as future work. Instead, we exploit additional properties in the 3-design to improve the bound.

Case (ii): t -designs with $t \geq 3$ To provide a uniform bound for all MPOs without the dependence on $\gamma(\boldsymbol{\rho}^*)$, we consider 3-designs, utilizing the property that uniform sampling from a 3-design mimics the first six moments of sampling uniformly according to the Haar measure. The following result establishes an improved guarantee for estimating MPO with δ -approximate t -designs ($t \geq 3$).

⁵Similar result also holds when \mathbf{u} is randomly generated from the unit sphere according to the Haar measure.

⁶For a random variable X , its subgaussian norm and subexponential norm are respectively defined as $\|X\|_{\psi_2} = \inf\{t > 0, \mathbb{E} e^{\frac{|X|^2}{t^2}} \leq 2\}$ and $\|X\|_{\psi_1} = \inf\{t > 0, \mathbb{E} e^{\frac{|X|}{t}} \leq 2\}$.

Theorem 2 (Stable recovery with 3-designs). *Suppose $\{\mathbf{A}_1, \dots, \mathbf{A}_K\}$ form a set of δ -approximate t -design POVMs ($t \geq 3$) and $\rho^* \in \mathbb{C}^{d^n \times d^n}$ is an MPO state with ranks (r_1, \dots, r_{n-1}) . If we measure the state M times using the POVM, then with probability $1 - e^{-\Omega(nd^2\bar{r}^2 \log n)}$, the solution $\hat{\rho}$ of the constrained least squares (10) satisfies*

$$\|\hat{\rho} - \rho^*\|_F \lesssim \frac{d\bar{r}\sqrt{(1+\delta)n \log n}}{(1-\delta)\sqrt{M}}. \quad (18)$$

The proof is given in Appendix D. With exact or approximate spherical 3-design POVMs, Theorem 2 ensures a stable recovery of the ground-truth state when the number of state copies $M \geq \Omega(nd^2\bar{r}^2 \log n/\epsilon^2)$. Notably, this uniform guarantee is applied to all MPOs. It is worth noting that the n -qubit Clifford group comprises a unitary (not spherical) 3-design POVM [68–70]. Sampling Clifford circuits uniformly at random reproduces the first 3 moments of the full unitary group endowed with the Haar measure. Unfortunately, unitary 3-designs are not precisely equivalent to spherical 3-designs, thus we cannot efficiently construct spherical 3-designs. However, this work [71] demonstrates one method to generate spherical 3-designs by extracting them from unitary designs. On the other hand, the SIC-POVM is not a 3-design POVM, hence the assumption of “uniformly” distributed probabilities may be indispensable.

We conclude this section by two additional remarks. First, the recovery guarantee (17) is established in the Frobenius norm rather than the trace norm. Nonetheless, if the MPO state ρ^* has a low matrix rank, we can also establish a recovery guarantee in the trace norm by utilizing a bound between trace distance and Hilbert-Schmidt distance for low-rank states, as proposed in [72]: $\|\hat{\rho} - \rho^*\|_1 \leq 2\sqrt{\text{rank}(\rho^*)}\|\hat{\rho} - \rho^*\|_F$. While this approach may provide a vacuous bound for high matrix ranks, we conjecture that the results in Theorem 1 and Theorem 2 can be extended for the trace norm, irrespective of the matrix rank of ρ^* , through direct analysis. However, we leave this as a topic for future work.

Second, while the solution $\hat{\rho}$ of (10) may be non-physical, we can impose additional PSD constraint to obtain a physical state without compromising the recovery guarantee in Theorem 1. Alternatively, we can simply project $\hat{\rho}$ onto the set of physical states $\mathbb{S}_+ := \{\rho \in \mathbb{C}^{d^n \times d^n} : \rho \succeq \mathbf{0}, \text{trace}(\rho) = 1\}$. Denote by $P_{\mathbb{S}_+}$ the projection onto the set \mathbb{S}_+ , which can be efficiently computed by projecting the eigenvalues onto a simplex [73]. Since the set \mathbb{S}_+ is convex, the corresponding projector is non-expansive, and hence

$$\|P_{\mathbb{S}_+}(\hat{\rho}) - \rho^*\|_F = \|P_{\mathbb{S}_+}(\hat{\rho}) - P_{\mathbb{S}_+}(\rho^*)\|_F \leq \|\hat{\rho} - \rho^*\|_F \leq \epsilon, \quad (19)$$

which implies that the projection step ensures that the state becomes physically valid while preserving or even improving the recovery guarantee.

4 Projected Gradient Descent with Guaranteed Convergence

In the literature of tensor recovery for tensor train (TT) format tensors, several iterative algorithms [74–78] have been proposed and analyzed from random measurements. While these algorithms can be applied to MPO by rewriting MPO as TT⁷, the analysis has predominantly focused on real-valued tensors with either clear measurements or corrupted by Gaussian noise. Thus, the guarantees cannot be directly applied to QST involving complex-valued MPOs and statistical noise induced by the empirical measurements that follow a multinomial distribution. In this section, we propose an iterative optimization algorithm and study its convergence for solving the constrained least-squares problem (10) that minimizes the discrepancy between the empirical measurements $\hat{\rho}$ and the linear mapping of the estimated MPO ρ .

We begin by reiterating the loss function in (10):

$$\min_{\rho \in \mathbb{X}_r} g(\rho) = \|\mathcal{A}(\rho) - \hat{\rho}\|_2^2. \quad (21)$$

We solve this constrained optimization problem by a projected gradient descent (PGD) that iteratively updates

$$\rho^{(\tau+1)} = \mathcal{P}_{\mathbb{X}_r}(\rho^{(\tau)} - \mu \nabla g(\rho^{(\tau)})), \quad (22)$$

⁷To establish the equivalence, we first reshape ρ into an n -th order tensor \mathcal{X} of size $d^2 \times d^2 \times \dots \times d^2$, where each pair (i_ℓ, j_ℓ) is mapped to a single index $s_\ell = i_\ell + d(j_\ell - 1)$ for $\ell = 1, \dots, n$. Consequently, the (s_1, \dots, s_n) -th element of \mathcal{X} becomes

$$\mathcal{X}(s_1, \dots, s_n) = \rho(i_1 \dots i_n, j_1 \dots j_n) = \mathbf{X}_1^{s_1} \mathbf{X}_2^{s_2} \dots \mathbf{X}_n^{s_n}, \quad (20)$$

where with abuse of notation we denote by $\mathbf{X}_\ell^{s_\ell} = \mathbf{X}_\ell^{i_\ell, j_\ell}$.

where μ is the step size, $\nabla g(\boldsymbol{\rho}^{(\tau)}) = \sum_{k=1}^K (\langle \mathbf{A}_k, \boldsymbol{\rho}^{(\tau)} \rangle - \widehat{p}) \mathbf{A}_k$ is the Wirtinger gradient⁸, and $\mathcal{P}_{\mathbb{X}_r}(\cdot)$ is the projection onto the set \mathbb{X}_r .

Since computing the optimal projection onto the set of TT format tensors is already known as NP-hard [40], computing the optimal projection onto the set \mathbb{X}_r is challenging even ignoring the constraint on the trace. Here, we use a two-step approximate projection $\mathcal{P}_{\mathbb{X}_r}(\cdot) = \mathcal{P}_{\text{trace}=1}(\text{SVD}_r^{tt}(\cdot))$, where $\text{SVD}_r^{tt}(\cdot)$ denotes the TT-SVD operation [27] that can compute an MPO (may not have trace 1) approximation for a given density matrix⁹, and $\mathcal{P}_{\text{trace}=1}(\cdot)$ represents the projection onto the convex set $\{\boldsymbol{\rho} \in \mathbb{C}^{d^n \times d^n} : \text{trace}(\boldsymbol{\rho}) = 1\}$ to have unit trace¹⁰. While the TT-SVD operation $\text{SVD}_r^{tt}(\cdot)$ may not produce an optimal approximation, it can be approved to be sub-optimal. In particular, for any density matrix $\boldsymbol{\rho}$, we have [27] $\|\text{SVD}_r^{tt}(\boldsymbol{\rho}) - \boldsymbol{\rho}\|_F^2 \leq (n-1) \min_{\boldsymbol{\rho}' \in \mathbb{X}_r} \|\boldsymbol{\rho}' - \boldsymbol{\rho}\|_F^2$. Moreover, the following result provides an improved bound when $\boldsymbol{\rho}$ can be approximated by an MPO.

Lemma 4. ([80, Lemma 26]) *Let $\boldsymbol{\rho}^* \in \mathbb{C}^{d^n \times d^n}$ be an MPO with ranks (r_1, \dots, r_{n-1}) . Denote by $\underline{\sigma}(\boldsymbol{\rho}^*)$ the smallest TT singular value of $\boldsymbol{\rho}^*$ ¹¹. Then for any perturbation $\mathbf{E} \in \mathbb{C}^{d^n \times d^n}$ with $C_n \|\mathbf{E}\|_F \leq \underline{\sigma}(\boldsymbol{\rho}^*)$ for some constant $C_n \geq 500n$, we have*

$$\|\text{SVD}_r^{tt}(\boldsymbol{\rho}^* + \mathbf{E}) - \boldsymbol{\rho}^*\|_F^2 \leq \|\mathbf{E}\|_F^2 + \frac{600n \|\mathbf{E}\|_F^3}{\underline{\sigma}(\boldsymbol{\rho}^*)}. \quad (23)$$

Local convergence of PGD We now provide convergence analysis for the PGD in (22). Without loss of generality, our analysis will be presented for the general δ -approximate t -design POVM. To unify results for both 2-designs and

3-designs, we define $\gamma_t(\boldsymbol{\rho}^*) = \begin{cases} \gamma(\boldsymbol{\rho}^*), & t = 2, \\ 1, & t > 2. \end{cases}$

Theorem 3 (Local linear convergence of PGD). *Suppose that $\{\mathbf{A}_1, \dots, \mathbf{A}_K\}$ form a set of δ -approximate t -design POVMs, which is used to measure an MPO state $\boldsymbol{\rho}^*$ M times. Given an initialization $\boldsymbol{\rho}^{(0)}$ satisfying*

$$\|\boldsymbol{\rho}^{(0)} - \boldsymbol{\rho}^*\|_F < \frac{\underline{\sigma}(\boldsymbol{\rho}^*)(d-1)(1-\delta)^2}{600n(1+\delta^2+(4d-2)\delta)}, \quad (24)$$

then with probability at least $1 - e^{-\Omega(nd^2\bar{r}^2 \log n)}$, the PGD in (22) with step size $\frac{\frac{600n}{\underline{\sigma}(\boldsymbol{\rho}^*)} \|\boldsymbol{\rho}^{(0)} - \boldsymbol{\rho}^*\|_F}{1 + \frac{600n}{\underline{\sigma}(\boldsymbol{\rho}^*)} \|\boldsymbol{\rho}^{(0)} - \boldsymbol{\rho}^*\|_F} \frac{K(d^n+1)}{d^n(1-\delta)} < \mu \leq \frac{(d-1)(d^n+1)(1-\delta)K}{(1+\delta)^2 d^{n+1}}$ generates iterates $\{\boldsymbol{\rho}^{(\tau)}\}$ that satisfy

$$\|\boldsymbol{\rho}^{(\tau)} - \boldsymbol{\rho}^*\|_F^2 \leq a^\tau \|\boldsymbol{\rho}^{(0)} - \boldsymbol{\rho}^*\|_F^2 + O\left(\frac{d\bar{r}(1-\delta)\sqrt{n\gamma_t(\boldsymbol{\rho}^*) \log n}}{(1+\delta)^{\frac{3}{2}}\sqrt{M}} \|\boldsymbol{\rho}^{(0)} - \boldsymbol{\rho}^*\|_F + \frac{(1-\delta)^2 \bar{r}^2 nd^2 \gamma_t(\boldsymbol{\rho}^*) \log n}{(1+\delta)^3 M}\right), \quad (25)$$

where $a = (1 + \frac{600n}{\underline{\sigma}(\boldsymbol{\rho}^*)} \|\boldsymbol{\rho}^{(0)} - \boldsymbol{\rho}^*\|_F)(1 - \frac{d^n(1-\delta)\mu}{K(d^n+1)}) < 1$.

The proof is given in Appendix E. The first term of the RHS of (25) decays at a linear rate with iteration number τ . Thus, Theorem 3 shows that with an appropriate initialization satisfying (24), PGD converges at a linear rate to a neighbor of $\boldsymbol{\rho}^*$ with a distance that scales as $\frac{d\bar{r}\underline{\sigma}(\boldsymbol{\rho}^*)\sqrt{\gamma_t(\boldsymbol{\rho}^*)}}{\sqrt{Mn}} + \frac{\bar{r}^2 nd^2 \gamma_t(\boldsymbol{\rho}^*)}{M}$ (where we plug in (24) and ignore the log terms and δ for the second term of RHS of (25)). Noting that $\underline{\sigma}(\boldsymbol{\rho}^*) \leq 1$, the recovery error is ensured to be small given that $M \gtrsim nd^2 \bar{r}^2 \gamma_t(\boldsymbol{\rho}^*)$, matching the results in Theorem 1 and Theorem 2.

⁸Note that $g(\boldsymbol{\rho})$ is non-holomorphic (i.e., not complex differentiable), which poses challenges for the development and analysis of standard gradient-based optimization algorithms. Fortunately, we can adopt Wirtinger gradient to extend the classical gradient concept to functions of complex variables [79]. In our context, we first parameterize the objective function as $g(\boldsymbol{\rho}, \boldsymbol{\rho}^*) = \sum_{k=1}^K (\langle \mathbf{A}_k^*, \boldsymbol{\rho}^* \rangle - \widehat{p}_K) (\langle \mathbf{A}_k, \boldsymbol{\rho} \rangle - \widehat{p}_K)$, and then compute the Wirtinger gradient $\nabla_{\boldsymbol{\rho}^*} g(\boldsymbol{\rho}, \boldsymbol{\rho}^*)$ by treating $\boldsymbol{\rho}$ and $\boldsymbol{\rho}^*$ as two independent variables. We can then use $\nabla_{\boldsymbol{\rho}^*} g(\boldsymbol{\rho}, \boldsymbol{\rho}^*)$ as the gradient in standard gradient-based optimization algorithms. To simplify the notation, we denote the Wirtinger gradient $\nabla_{\boldsymbol{\rho}^*} g(\boldsymbol{\rho}, \boldsymbol{\rho}^*)$ simply as $\nabla g(\boldsymbol{\rho})$.

⁹The output $\text{SVD}_r^{tt}(\mathbf{A})$ is always Hermitian if \mathbf{A} is Hermitian.

¹⁰This can be achieved by computing the eigendecomposition and subsequently projecting the eigenvalues onto the simplex [73]. While this process may increase the MPO ranks, our observations indicate that this increase is often minimal or does not occur. However, this process (particularly computing the eigendecomposition) could be computationally expensive for large quantum states. Alternatively, in our implementation, we simply use $\mathcal{P}_{\text{trace}=1}(\boldsymbol{\rho}) = \boldsymbol{\rho} / \text{trace}(\boldsymbol{\rho})$ which is computationally efficient while simultaneously preserving the MPO structure. Thus, in the analysis, we will assume the projection $\mathcal{P}_{\text{trace}=1}(\cdot)$ also preserves the MPO structure of the input.

¹¹Specifically, we reshape $\boldsymbol{\rho}$ into an n -th order tensor \mathcal{X} of size $d^2 \times d^2 \times \dots \times d^2$ and define the ℓ -th unfolding matrix of tensor \mathcal{X} as $\mathbf{X}^{(\ell)} \in \mathbb{C}^{d^{2\ell} \times d^{2n-2\ell}}$, where the $(s_1 \dots s_\ell, s_{\ell+1} \dots s_n)$ -th element of $\mathbf{X}^{(\ell)}$ is given by $\mathbf{X}^{(\ell)}(s_1 \dots s_\ell, s_{\ell+1} \dots s_n) = \mathcal{X}(s_1, \dots, s_n)$. With the ℓ -th unfolding matrix $\mathbf{X}^{(\ell)}$ and the ranks, we can obtain its smallest TT singular value $\underline{\sigma}(\mathcal{X}) = \min_{\ell=1}^{n-1} \sigma_{r_\ell}(\mathbf{X}^{(\ell)})$.

Spectral initialization We now discuss some potential initialization strategies for the PGD. A common approach to generating an appropriate initialization for signal estimation in nonconvex scenarios in the spectral initialization approach. It has been widely employed for various inverse problems [81], such as phase retrieval [82,83], low-rank matrix recovery [84,85], and structured tensor recovery [77,86,87]. In our context, this entails simply computing an MPO approximation to $\sum_{k=1}^K \frac{K(d^n+1)}{d^n} \hat{p}_k \mathbf{A}_k$, where $\sum_{k=1}^K \frac{K(d^n+1)}{d^n} \hat{p}_k \mathbf{A}_k$ is equivalent to apply the adjoint operator of \mathcal{A} on the empirical measurements $\hat{\mathbf{p}}$ with a scaling factor $K(d^n+1)/d^n$ that is used to balance the energy according to (7). Specifically, by using the same projection $\mathcal{P}_{\mathbb{X}_r}$ in the PGD, we can compute an initialization via

$$\boldsymbol{\rho}^{(0)} = \mathcal{P}_{\mathbb{X}_r} \left(\sum_{k=1}^K \frac{K(d^n+1)}{d^n} \hat{p}_k \mathbf{A}_k \right). \quad (26)$$

The following result ensures that the initialization $\boldsymbol{\rho}^{(0)}$ is close to $\boldsymbol{\rho}^*$.

Theorem 4. *Suppose that $\{\mathbf{A}_1, \dots, \mathbf{A}_K\}$ form a set of δ -approximate t -design POVMs, which is used to measure an MPO state $\boldsymbol{\rho}^*$ M times. By utilizing the spectral initialization in (26), with probability $1 - e^{-\Omega(nd^2\bar{r}^2 \log n)}$, we have*

$$\|\boldsymbol{\rho}^{(0)} - \boldsymbol{\rho}^*\|_F \leq (1 + \sqrt{n-1}) \cdot O \left(\frac{d\bar{r} \sqrt{(1+\delta)n\gamma_t(\boldsymbol{\rho}^*) \log n}}{\sqrt{M}} + \delta \|\boldsymbol{\rho}^*\|_F \right). \quad (27)$$

Its proof is given in Appendix F. The scaling term $\sqrt{n-1}$ arises due to the sub-optimal bound for the projection $\mathcal{P}_{\mathbb{X}_r}(\cdot)$. Recall that $\gamma_t(\boldsymbol{\rho}^*) = 1$ for all $\boldsymbol{\rho}^*$ when spherical 3-design POVMs (i.e., $t \geq 3$), and $\gamma_t(\boldsymbol{\rho}^*) = \gamma(\boldsymbol{\rho}^*)$ for spherical 2-design POVMs (i.e., $t = 2$). Theorem 4 shows that when $\gamma_t(\boldsymbol{\rho}^*)$ is small—true for all MPOs when using 3-designs and for those having relatively uniform probability distribution with 2-design POVMs—the spectral initialization provides a relatively good estimation with a polynomially large M . In particular, considering exact t -design POVMs or cases where δ is small, (27) ensures that $\|\boldsymbol{\rho}^{(0)} - \boldsymbol{\rho}^*\|_F^2$ scales in their order of $\frac{n^2 d^2 \bar{r}^2}{M}$ when ignoring the log terms and $\gamma_t(\boldsymbol{\rho}^*)$. Note that the requirements on the number of measurements are slightly more stringent than those in Theorem 1 and Theorem 2 due to the sub-optimal bound for the projection $\mathcal{P}_{\mathbb{X}_r}(\cdot)$. However, as will be illustrated in Section 5, our numerical experiments show that even a randomly initialized PGD can very efficiently find an estimate of the target state. A theoretical explanation for this phenomenon will be the focus of future research. We suspect that it may be possible to relax the requirement on the initialization in Theorem 3, or to demonstrate that PGD rapidly enters the region of local attraction, even if the random initialization starts outside of this region.

Projected stochastic gradient descent The primary computational complexity of the PGD (22) arises from computing the gradient, which involves an exponentially large number (K) of inner product operations between \mathbf{A}_k and $\boldsymbol{\rho}^{(\tau)}$, with a complexity of $O(Kd^{2n})$ by naive computation. When the POVMs $\{\mathbf{A}_k\}_{k=1}^K$ also have MPO representations, such as the local measurements as detailed in the subsequent section, the complexity of each inner product can be reduced to $O(n\bar{r}^3)$ from $O(d^{2n})$ by using the dot product method [27] for two MPOs. Similarly, the gradient update $\boldsymbol{\rho}^{(\tau)} - \mu \nabla g(\boldsymbol{\rho}^{(\tau)})$ in (22) can also be represented in the MPO form rather than as a full density matrix, allowing us to utilize TT-rounding to efficiently compute TT-SVD with polynomial computational complexity in n [27].

The issue of computing all the K inner products in one iteration can be addressed by using stochastic methods [88]. In our context, exploiting the fact that the empirical probabilities $\{\hat{p}_i\}$ are very sparse (at most M of them are nonzero) when the measured time M is much smaller than K , we can utilize a customized stochastic method. Specifically, unlike standard approaches that either randomly or sequentially select a subset of samples for computing gradient in each iteration, we can use the nonzero measurements more frequently. For instance, each time (often called epoch in machine learning), we first select a subset (say N) of empirical probabilities that include all the nonzero ones and a few numbers of zero ones (which can be either randomly selected or selected in a sequential), and then perform N/B iterations of PSGD with each iteration using B measurements selected sequentially from this subset.

5 Numerical experiments with local IC-POVMs

To our best knowledge, there are no known efficient implementations of SIC-POVM or spherical t -designs with $t \geq 2$ for a many-qubit system using local quantum circuits available in current or near-future quantum hardware. It is not

surprising that the sample-optimal measurement setting for recovering an MPO state is not efficiently implementable, as this is also the case for the QST of generic quantum states [17,18,20]. To make our results more experimentally relevant, in this section we consider a different type of IC-POVM that is efficiently implementable. Specifically, we consider the following local SIC-POVM $\{\mathbf{B}_i\}_{i=1}^4$ for each qubit

$$\left\{ \begin{bmatrix} \frac{1}{2} & 0 \\ 0 & 0 \end{bmatrix}, \begin{bmatrix} \frac{1}{6} & \frac{\sqrt{2}}{6} \\ \frac{\sqrt{2}}{6} & \frac{1}{6} \end{bmatrix}, \begin{bmatrix} \frac{1}{6} & \frac{\sqrt{2}}{6} e^{-i\frac{2\pi}{3}} \\ \frac{\sqrt{2}}{6} e^{i\frac{2\pi}{3}} & \frac{1}{6} \end{bmatrix}, \begin{bmatrix} \frac{1}{6} & \frac{\sqrt{2}}{6} e^{-i\frac{4\pi}{3}} \\ \frac{\sqrt{2}}{6} e^{i\frac{4\pi}{3}} & \frac{1}{6} \end{bmatrix} \right\}. \quad (28)$$

We can then generate the set of IC-POVM for an n -qubit system as $\{\mathbf{A}_i\}_{i=1}^{4^n} = \{\mathbf{B}_{i_1} \otimes \cdots \otimes \mathbf{B}_{i_n}\}_{i_1, \dots, i_n}$. Importantly, such IC-POVM has been recently demonstrated experimentally using trapped ions in a scalable way [89] and can be implemented in most quantum computing hardware platforms using either ancilla qubits or extra low-energy states in the physical carriers of the qubits.

While our main results (Theorems 1 and 2) do not apply to such a measurement setting, we show that certain MPO states can be recovered using this IC-POVM using a number of state copies only linear in n and the PGD and PSGD algorithms developed in Section 3. A more systematic study on what types of MPO states can be recovered efficiently using the local IC-POVM can be found in [90], using a different optimization algorithm based on maximal likelihood estimation (MLE). As an example, here we consider a random matrix product density operator (MPDO) state [65] of the following form (1), i.e, the $(i_1 \cdots i_n, j_1 \cdots j_n)$ -th entry of ρ^* can be generated by

$$\rho^*(i_1 \cdots i_n, j_1 \cdots j_n) = \mathbf{X}_1^{*i_1, j_1} \mathbf{X}_2^{*i_2, j_2} \cdots \mathbf{X}_n^{*i_n, j_n}. \quad (29)$$

To ensure ρ^* PSD, we generate each matrix $\mathbf{X}_\ell^{*i_\ell, j_\ell}$ as [65]

$$\mathbf{X}_\ell^{*i_\ell, j_\ell} = \sum_{a_\ell=1}^{K_\ell} \mathbf{A}_\ell^{*i_\ell, a_\ell} \otimes (\mathbf{A}_\ell^{*j_\ell, a_\ell})^*, \quad (30)$$

where the symbol $*$ represents the complex conjugate, \otimes denotes the Kronecker product, K_ℓ is an arbitrary positive integer that controls purity of the generated state, and each matrix $\mathbf{A}_\ell^{*i_\ell, a_\ell}$ has dimension $\kappa \times \kappa$, except for $\mathbf{A}_1^{*i_1, a_1}$ and $\mathbf{A}_n^{*i_n, a_n}$, which are of dimension $1 \times \kappa$ and $\kappa \times 1$ respectively. Each entry of $\mathbf{A}_\ell^{*i_\ell, a_\ell}$ is i.i.d. randomly generated with both its real and imaginary parts drawn uniformly from the interval $[-1, 1]$. In the experiments, we set $K_\ell = 10$ to ensure the state is sufficiently mixed; using $K_\ell = 1$ would generate a pure state. The generated ρ^* is an MPO with a bond dimension of $\bar{\tau} = \kappa^2$ and is always PSD. To be a physical state, ρ^* also needs to have unit trace, which can be done by calculating

$$\text{trace}(\rho^*) = (\mathbf{X}_1^{*1,1} + \mathbf{X}_1^{*2,2}) \cdots (\mathbf{X}_n^{*1,1} + \mathbf{X}_n^{*2,2}), \quad (31)$$

and then dividing each matrix $\mathbf{X}_\ell^{*i_\ell, j_\ell}$ by $(\text{trace}(\rho^*))^{\frac{1}{n}}$.

In order to validate the theoretical analysis presented in the preceding sections, we apply PGD and PSGD with spectral initialization across various measurements. To further mitigate the high computational complexity of the spectral method, we will also use a random initialization generated by a random MPDO as the starting point for both PGD and PSGD. This approach is motivated by our observation that random initialization, when the target is a random MPDO, can effectively serve as a convergence-guaranteeing initialization.

Performance of PGD In the first set of experiments, we set $M = 3000$ for empirical measurements. Since we will perform experiments for different number of qubits, we employ PGD with diminishing step sizes $\mu_\tau = \mu_0 \cdot 2^n \cdot \lambda^\tau$ (with $\lambda = 0.9$), which is found to provide stable performance across varying n . When a random initialization is used, we set $\mu_0 = \frac{5}{4}$ for $\bar{\tau} = 1$ and $\mu_0 = \frac{5}{8}$ for $\bar{\tau} = 4$. As for spectral initialization, μ_0 is set to $\frac{5}{8}$ for $\bar{\tau} = 1$ and $\frac{5}{16}$ for $\bar{\tau} = 4$. Figure 1(a) depicts the recovery error as a function of n for various $\bar{\tau}$ and initialization methods. As anticipated, the recovery error tends to rise with an increase in $\bar{\tau}$, yet the PGD algorithm displays stability across all cases. Notably, we observe that the recovery error increases only polynomially rather than exponentially with respect to n , aligning with the findings in Theorems 1 and 2. Furthermore, Figure 1(b) illustrates the convergence behavior of PGD with both spectral and random initializations. As n increases, the quality of initial values from spectral initialization deteriorates,

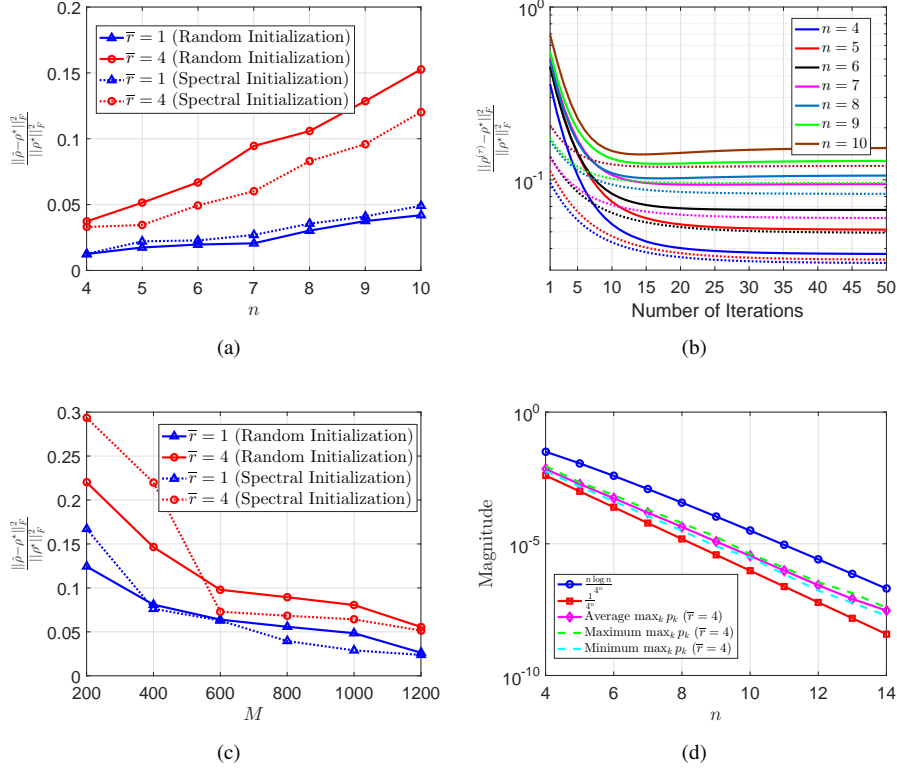


Figure 1: Illustration of (a) recovery error for different initialization methods, \bar{r} and n with $M = 3000$; (b) convergence rate of PGD for different n , spectral initialization (dotted lines), and random initialization (solid lines) with $M = 3000$ and $\bar{r} = 4$; (c) recovery error with $n = 5$ for different initialization methods, \bar{r} and M ; (d) p_{\max} for the MPDO.

aligning with the theoretical analysis presented in Theorem 4. Conversely, although the recovery error with random initialization is slightly worse than that of the spectral method, it offers a reliable starting point for stable recovery while avoiding the high computational complexity associated with the spectral method. Subsequently, we evaluate the recovery performance across varying values of M , selecting $\mu_0 = \frac{5}{32}$ for random initialization and $\mu_0 = \frac{1}{16}$ for spectral initialization, with $\lambda = 1$. In Figure 1(c), we observe that the recovery performance of PGD with spectral and random initializations is comparable, with improved recovery error as M increases. Finally, Figure 1(d) reveals that the numerator of the average maximum probability is polynomial, ensuring the effectiveness of the assumption.

Performance comparison between PGD and PSGD In the second experiment, we compare the performance of PGD and PSGD in estimating the MPDO. We set $M = 3000$ and $\bar{r} = 4$. We use the same setting for PGD in Figure 1(a) and use diminishing step sizes $\mu_\tau = \frac{5}{4} \times 2^n \times 0.9^\tau$ for random initialization and $\mu_\tau = 10 \times 0.9^\tau$ for spectral initialization. Additionally, we choose $N = 10 \times 4n\bar{r}^2 = 640n$ measurements in one epoch and $B = 32$ in each iteration of one epoch. Figure 2(a) provides an analysis of the convergence properties of PSGD with random initialization, demonstrating that this achieves a linear convergence rate and exhibits stable recovery errors as n increases. Furthermore, due to its polynomial computational complexity, PSGD with random initialization is viable for systems with up to 14 qubits. In Figure 2(b), we observe that PSGD with random initialization delivers performance comparable to that achieved with spectral initialization. Notably, although PSGD with polynomial measurements incurs a marginally higher recovery error compared to PGD, it nonetheless achieves a stable recovery error that grows polynomially with n .

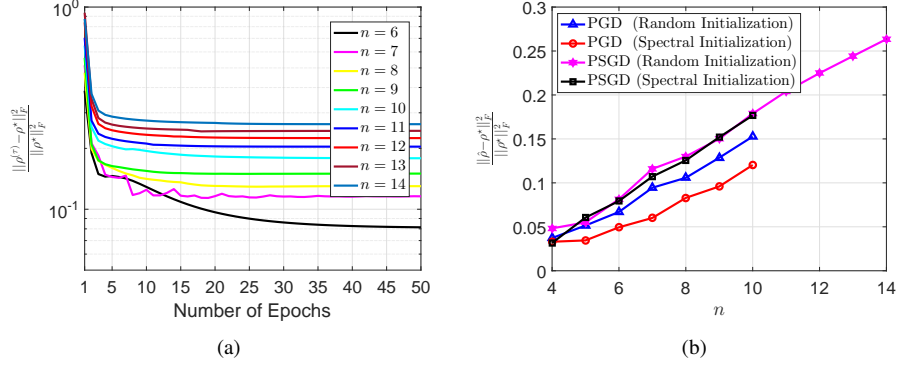


Figure 2: (a) Convergence comparison of PSGD with random initialization for various n ; (b) Performance comparison between PGD and PSGD with random and spectral initializations.

6 Conclusion

This paper focuses on the sample complexity bounds for recovering structured quantum states in one-dimension that are represented as matrix product operators (MPOs) with finite bond dimensions. The study begins by establishing theoretical bounds on the accuracy of a constrained least-squares estimator for MPO state recovery, utilizing empirical measurements from a class of Informationally Complete Positive Operator-Valued Measure (IC-POVM). The results indicate that assuming probabilities measured by one POVM are approximately uniform for SIC-POVM or 2-designs, or without any assumption for t -designs ($t \geq 3$), a stable recovery guarantee requires the number of state copies to be only linear in the the number of qudits n and is thus sample optimal. Additionally, the paper introduces a provable projected gradient descent (PGD) algorithm. It demonstrates that, with appropriate initialization achievable through spectral initialization, PGD converges to the neighborhood of the target state at a linear rate and achieves an error bound scaling only linear in n . These results address fundamental questions on whether quantum states with efficient classical representations can be recovered efficiently. While the measurement settings used in our sample complexity bounds are not efficiently implementable, we show that certain MPO states may be recovered efficiently using a local IC-POVM that can be experimentally achieved on current quantum hardware. It remains an open question what class of MPO states, or other structured quantum states, can be recovered not only using an efficient number of state copies, but also using an efficiently implementable measurement setting [90].

Acknowledgment

We acknowledge funding support from NSF Grants No. CCF-1839232, PHY-2112893, CCF-2106834 and CCF-2241298, as well as the W. M. Keck Foundation. We thank the Ohio Supercomputer Center for providing the computational resources needed in carrying out this work.

Appendices

A Proof of Lemma 1

Proof. According to [91], any Hermitian matrix $\rho \in \mathbb{C}^{d^n \times d^n}$ can be represented in terms of elements of the dual basis as

$$\rho = \sum_{k=1}^{d^{2n}} \langle A_k, \rho \rangle \tilde{A}_k. \quad (32)$$

Here, the dual basis $\{\tilde{\mathbf{A}}_k\}$ is a basis such that $\langle \mathbf{A}_k, \tilde{\mathbf{A}}_j \rangle = \begin{cases} 1, & k = j \\ 0, & k \neq j \end{cases}$. For a general SIC-POVM $\{\mathbf{A}_k\}$, the dual basis is comprised by operators [92]

$$\tilde{\mathbf{A}}_k = d^n(d^n + 1)\mathbf{A}_k - \mathbf{I}_{d^n}. \quad (33)$$

Using ρ in (32), we have

$$\begin{aligned} \text{trace}(\rho^2) &= (d^n(d^n + 1) - 1)\|\mathcal{A}(\rho)\|_2^2 - \sum_{j \neq k} \langle \mathbf{A}_j, \rho \rangle \langle \mathbf{A}_k, \rho \rangle \\ &= (d^n(d^n + 1) - 1)\|\mathcal{A}(\rho)\|_2^2 - \left(\left(\sum_{i=1}^{d^{2n}} \langle \mathbf{A}_i, \rho \rangle \right)^2 - \|\mathcal{A}(\rho)\|_2^2 \right) \\ &= d^n(d^n + 1)\|\mathcal{A}(\rho)\|_2^2 - (\text{trace}(\rho))^2, \end{aligned} \quad (34)$$

where the first line follows (22) in [91, Proposition 1]. In addition, due to $\rho = \rho^\dagger$, we have $\text{trace}(\rho^2) = \text{trace}(\rho^\dagger \rho) = \|\rho\|_F^2$. This completes the proof. \square

B Proof of Lemma 2

Proof. According to [39, Theorem 1] and Lemma 5, we have

$$\int (\mathbf{w}\mathbf{w}^\dagger)^{\otimes 2} d\mathbf{w} = \frac{\mathbf{I} + \mathbf{S}}{d^n(d^n + 1)}, \quad (35)$$

where \mathbf{S} is the swap operator. Taking the inner product between (35) and $\frac{d^{2n}}{K}\rho^{\otimes 2}$ we get

$$\begin{aligned} \left\langle \int (\mathbf{w}\mathbf{w}^\dagger)^{\otimes 2} d\mathbf{w}, \frac{d^{2n}}{K}\rho^{\otimes 2} \right\rangle &= \frac{d^n(\text{trace}(\rho^{\otimes 2}) + \text{trace}(\mathbf{S}\rho^{\otimes 2}))}{K(d^n + 1)} \\ &= \frac{d^n((\text{trace}(\rho))^2 + \text{trace}(\rho^2))}{K(d^n + 1)} \\ &= \frac{d^n((\text{trace}(\rho))^2 + \|\rho\|_F^2)}{K(d^n + 1)}, \end{aligned} \quad (36)$$

where the penultimate line follows $\text{trace}(\mathbf{S}\rho^{\otimes 2}) = \text{trace}(\rho^2)$ [16, Lemma 17] for any Hermitian matrix ρ . Based on $\text{trace}((\mathbf{w}_k\mathbf{w}_k^\dagger)^{\otimes 2}(\rho^{\otimes 2})) = \text{trace}((\mathbf{w}_k\mathbf{w}_k^\dagger\rho) \otimes (\mathbf{w}_k\mathbf{w}_k^\dagger\rho)) = (\text{trace}(\mathbf{w}_k\mathbf{w}_k^\dagger\rho))^2$, this completes the proof. \square

C Proof of Theorem 1

Proof. Now, we start by upper-bounding $\langle \boldsymbol{\eta}, \mathcal{A}(\hat{\rho} - \rho^*) \rangle$. Towards that goal, we first rewrite this term as

$$\langle \boldsymbol{\eta}, \mathcal{A}(\hat{\rho} - \rho^*) \rangle = \sum_{k=1}^K \eta_k \langle \mathbf{A}_k, (\hat{\rho} - \rho^*) \rangle \leq \|\hat{\rho} - \rho^*\|_F \max_{\rho \in \overline{\mathbb{X}}_{2r}} \sum_{k=1}^K \eta_k \langle \mathbf{A}_k, \rho \rangle, \quad (37)$$

where we denote by $\overline{\mathbb{X}}_r$ the normalized set of MPOs with $\mathbf{r} = [r_1, \dots, r_{n-1}]$:

$$\begin{aligned} \overline{\mathbb{X}}_r &= \left\{ \rho \in \mathbb{C}^{d^n \times d^n} : \rho = \rho^\dagger, \|\rho\|_F \leq 1, \text{trace}(\rho) = 0, \rho(i_1 \cdots i_n, j_1 \cdots j_n) = \mathbf{X}_1^{i_1, j_1} \mathbf{X}_2^{i_2, j_2} \cdots \mathbf{X}_n^{i_n, j_n}, \right. \\ &\quad \left. \mathbf{X}_\ell^{i_\ell, j_\ell} \in \mathbb{C}^{r_{\ell-1} \times r_\ell}, \ell \in [n-1], r_0 = r_n = 1 \right\}. \end{aligned} \quad (38)$$

It is important to highlight that in comparison to \mathbb{X}_r in (11), $\overline{\mathbb{X}}_r$ additionally includes $\|\rho\|_F \leq 1$ and $\text{trace}(\rho) = 0$.

The rest of the proof is to bound $\max_{\rho} \sum_{k=1}^K \eta_k \langle \mathbf{A}_k, \rho \rangle$, which will be achieved by using a covering argument. First, when conditioned on \mathbf{A}_k , we consider any fixed value of $\rho^{(p)} = [\mathbf{X}_1^{(p_1)}, \dots, \mathbf{X}_n^{(p_n)}] \in \overline{\mathbb{X}}_{2r}$ and according to [1, Appendix B-A], construct a ξ -net $\{\rho^{(1)}, \dots, \rho^{(N_1 \cdots N_n)}\} = \{[\mathbf{X}_1^{(1)}, \dots, \mathbf{X}_n^{(1)}], \dots, [\mathbf{X}_1^{(N_1)}, \dots, \mathbf{X}_n^{(N_n)}]\}$ such that $\sup_{\mathbf{X}_\ell: \|\mathbf{X}_\ell\|_F \leq 1} \min_{p_\ell \leq N_\ell} \|\mathbf{X}_\ell - \mathbf{X}_\ell^{(p_\ell)}\|_F \leq \xi$, $\ell = 1, \dots, n$ with covering number $\Pi_{\ell=1}^n N_\ell \leq \left(\frac{4+\xi}{\xi}\right)^{8r_1 + \sum_{i=2}^{n-1} 16r_{i-1}r_i + 8r_{n-1}}$.

Then we apply Lemma 3 to establish a concentration inequality for the expression $\sum_{k=1}^K \eta_k \langle \mathbf{A}_k, \rho^{(p)} \rangle$ as follows:

$$\begin{aligned} \mathbb{P}\left(\sum_{k=1}^K \eta_k \langle \mathbf{A}_k, \rho^{(p)} \rangle \geq t\right) &\leq e^{-\frac{Mt}{4 \max_k |\langle \mathbf{A}_k, \rho^{(p)} \rangle|}} \min\left\{1, \frac{\max_k |\langle \mathbf{A}_k, \rho^{(p)} \rangle| t}{4 \sum_{k=1}^K \langle \mathbf{A}_k, \rho^{(p)} \rangle^2 p_k}\right\} + e^{-\frac{Mt^2}{8 \sum_{k=1}^K \langle \mathbf{A}_k, \rho^{(p)} \rangle^2 p_k}} \\ &\leq e^{-\frac{Mt^2}{16 \sum_{k=1}^K \langle \mathbf{A}_k, \rho^{(p)} \rangle^2 p_k}} + e^{-\frac{Mt^2}{8 \sum_{k=1}^K \langle \mathbf{A}_k, \rho^{(p)} \rangle^2 p_k}}, \end{aligned} \quad (39)$$

where without loss of generality, we assume that $\frac{\max_k |\langle \mathbf{A}_k, \rho^{(p)} \rangle| t}{4 \sum_{k=1}^K \langle \mathbf{A}_k, \rho^{(p)} \rangle^2 p_k} \leq 1$ in the last line.

Since $\sum_{k=1}^K \langle \mathbf{A}_k, \rho^{(p)} \rangle^2 \leq \frac{(1+\delta)d^n}{K(d^n+1)}$ from Lemma 2 and $\max_k p_k = \frac{\gamma(\rho^*)}{K}$, we can derive $\sum_{k=1}^K \langle \mathbf{A}_k, \rho^{(p)} \rangle^2 p_k \leq \frac{(1+\delta)d^n \gamma(\rho^*)}{K^2(d^n+1)}$ and thus, have

$$\mathbb{P}\left(\sum_{k=1}^K \eta_k \langle \mathbf{A}_k, \rho^{(p)} \rangle \geq t\right) \leq 2e^{-\frac{K^2(d^n+1)Mt^2}{16(1+\delta)d^n\gamma(\rho^*)}}. \quad (40)$$

According to the same analysis of [1, eq.(110)] with the covering number $\left(\frac{4+\xi}{\xi}\right)^{8r_1 + \sum_{i=2}^{n-1} 16r_{i-1}r_i + 8r_{n-1}}$, we can derive

$$\begin{aligned} \mathbb{P}\left(\sum_{k=1}^K \eta_k \langle \mathbf{A}_k, \rho \rangle \geq t\right) &\leq \mathbb{P}\left(\sum_{k=1}^K \eta_k \langle \mathbf{A}_k, \rho^{(p)} \rangle \geq \frac{t}{2}\right) \\ &\leq \left(\frac{4+\xi}{\xi}\right)^{8r_1 + \sum_{i=2}^{n-1} 16r_{i-1}r_i + 8r_{n-1}} e^{-\frac{K^2(d^n+1)Mt^2}{16(1+\delta)d^n\gamma(\rho^*)} + \log 2} \\ &\leq e^{-\frac{K^2(d^n+1)Mt^2}{16(1+\delta)d^n\gamma(\rho^*)} + Cnd^2\bar{r}^2 \log n + \log 2}, \end{aligned} \quad (41)$$

where the first equation follows [1, eq.(89)] with $\xi = \frac{1}{2n}$, $\bar{r} = \max_i r_i$, and C is a universal constant in the last line.

By taking $t = \frac{c_1 d \bar{r} \sqrt{(1+\delta)nd^n\gamma(\rho^*) \log n}}{K \sqrt{(d^n+1)M}}$ in the above equation, we further obtain

$$\mathbb{P}\left(\sum_{k=1}^K \eta_k \langle \mathbf{A}_k, \rho \rangle \leq \frac{c_1 d \bar{r} \sqrt{(1+\delta)nd^n\gamma(\rho^*) \log n}}{K \sqrt{(d^n+1)M}}\right) \geq 1 - e^{-c_2 nd^2 \bar{r}^2 \log n}, \quad (42)$$

where c_1 and c_2 are constants.

Hence, with (37), we can obtain

$$\langle \eta, \mathcal{A}(\hat{\rho} - \rho^*) \rangle \leq \frac{c_1 d \bar{r} \sqrt{(1+\delta)nd^n\gamma(\rho^*) \log n}}{K \sqrt{(d^n+1)M}} \|\hat{\rho} - \rho^*\|_F. \quad (43)$$

Combing (13) and (14), with probability $1 - e^{-c_2 nd^2 \bar{r}^2 \log n}$, we arrive at

$$\|\hat{\rho} - \rho^*\|_F \leq \frac{c_3 d \bar{r} \sqrt{(1+\delta)n\gamma(\rho^*) \log n}}{(1-\delta)\sqrt{M}}, \quad (44)$$

where c_3 is a constant. \square

D Proof of Theorem 2

Proof. Firstly, we derive the upper bound of $\sum_{k=1}^K \langle \mathbf{A}_k, \boldsymbol{\rho} - \boldsymbol{\rho}^* \rangle^2 p_k$ for $\boldsymbol{\rho}, \boldsymbol{\rho}^* \in \mathbb{X}_r$ in (11). Leveraging the ties of δ -approximate 3-designs [39,64] and Lemma 5, we can get:

$$\begin{aligned} \sum_{k=1}^K \langle \mathbf{A}_k, \boldsymbol{\rho} - \boldsymbol{\rho}^* \rangle^2 p_k &= \sum_{k=1}^K \langle \frac{d^n}{K} \mathbf{w}_k \mathbf{w}_k^\dagger, \boldsymbol{\rho} - \boldsymbol{\rho}^* \rangle^2 \langle \frac{d^n}{K} \mathbf{w}_k \mathbf{w}_k^\dagger, \boldsymbol{\rho}^* \rangle \\ &= \sum_{k=1}^K \frac{8^n}{K^3} \text{trace}((\mathbf{w}_k \mathbf{w}_k^\dagger)^{\otimes 3} (\boldsymbol{\rho} - \boldsymbol{\rho}^*) \otimes (\boldsymbol{\rho} - \boldsymbol{\rho}^*) \otimes \boldsymbol{\rho}^*) \\ &\leq \frac{d^{3n}}{K^2} \frac{6(1+\delta)}{(d^n+2)(d^n+1)d^n} \text{trace}(\mathcal{P}_{\text{sym}^{\otimes 3}}(\boldsymbol{\rho} - \boldsymbol{\rho}^*) \otimes (\boldsymbol{\rho} - \boldsymbol{\rho}^*) \otimes \boldsymbol{\rho}^*), \end{aligned} \quad (45)$$

where $\mathcal{P}_{\text{sym}^{\otimes 3}}$, defined in [39, Lemma 3], represents the projector onto the symmetric subspace. Additionally, based on [60, Lemma 7] and [93, eq. (322)], we have

$$\begin{aligned} &\text{trace}(\mathcal{P}_{\text{sym}^{\otimes 3}}(\boldsymbol{\rho} - \boldsymbol{\rho}^*) \otimes (\boldsymbol{\rho} - \boldsymbol{\rho}^*) \otimes \boldsymbol{\rho}^*) \\ &= \frac{1}{6} \left((\text{trace}(\boldsymbol{\rho} - \boldsymbol{\rho}^*))^2 \text{trace}(\boldsymbol{\rho}^*) + \text{trace}((\boldsymbol{\rho} - \boldsymbol{\rho}^*)^2) \text{trace}(\boldsymbol{\rho}^*) \right. \\ &\quad \left. + 2 \text{trace}((\boldsymbol{\rho} - \boldsymbol{\rho}^*) \boldsymbol{\rho}^*) \text{trace}(\boldsymbol{\rho} - \boldsymbol{\rho}^*) + 2 \text{trace}((\boldsymbol{\rho} - \boldsymbol{\rho}^*)^2 \boldsymbol{\rho}^*) \right) \\ &= \frac{1}{6} \|\boldsymbol{\rho} - \boldsymbol{\rho}^*\|_F^2 + \frac{1}{3} \text{trace}((\boldsymbol{\rho} - \boldsymbol{\rho}^*)^2 \boldsymbol{\rho}^*). \end{aligned} \quad (46)$$

Note that this can also be directly obtained from [94, eq. (S36)] when $\text{trace}(\boldsymbol{\rho} - \boldsymbol{\rho}^*) = 0$. Consequently, we arrive at $\sum_{k=1}^K \langle \mathbf{A}_k, \boldsymbol{\rho} - \boldsymbol{\rho}^* \rangle^2 p_k \leq O\left(\frac{(1+\delta) \|\boldsymbol{\rho} - \boldsymbol{\rho}^*\|_F^2 + \text{trace}((\boldsymbol{\rho} - \boldsymbol{\rho}^*)^2 \boldsymbol{\rho}^*)}{K^2}\right)$. Given that $\boldsymbol{\rho} - \boldsymbol{\rho}^*$ is Hermitian, we can ensure $(\boldsymbol{\rho} - \boldsymbol{\rho}^*)^2 = (\boldsymbol{\rho} - \boldsymbol{\rho}^*)(\boldsymbol{\rho} - \boldsymbol{\rho}^*)^\dagger$ is PSD. Building upon [95, Theorem 1] using two PSD matrices $(\boldsymbol{\rho} - \boldsymbol{\rho}^*)^2$ and $\boldsymbol{\rho}^*$, we further deduce $\text{trace}((\boldsymbol{\rho} - \boldsymbol{\rho}^*)^2 \boldsymbol{\rho}^*) \leq \text{trace}((\boldsymbol{\rho} - \boldsymbol{\rho}^*)^2) \text{trace}(\boldsymbol{\rho}^*) = \|\boldsymbol{\rho} - \boldsymbol{\rho}^*\|_F^2$. Ultimately, we obtain

$$\sum_{k=1}^K \langle \mathbf{A}_k, \boldsymbol{\rho} - \boldsymbol{\rho}^* \rangle^2 p_k \leq O\left(\frac{(1+\delta) \|\boldsymbol{\rho} - \boldsymbol{\rho}^*\|_F^2}{K^2}\right). \quad (47)$$

Applying the same analysis as in Appendix C, we can derive

$$\mathbb{P}\left(\max_{\boldsymbol{\rho} \in \overline{\mathbb{X}}_{2r}} \sum_{k=1}^K \eta_k \langle \mathbf{A}_k, \boldsymbol{\rho} \rangle \leq \frac{c_1 d \bar{r} \sqrt{(1+\delta)n \log n}}{K \sqrt{M}}\right) \geq 1 - e^{-c_2 n d^2 \bar{r}^2 \log n}, \quad (48)$$

where $\overline{\mathbb{X}}_{2r}$ is defined in (38) and c_1, c_2 are constants.

Combing (13), (14) and (48), we can conclude:

$$\|\hat{\boldsymbol{\rho}} - \boldsymbol{\rho}^*\|_F \leq O\left(\frac{d \bar{r} \sqrt{(1+\delta)n \log n}}{(1-\delta) \sqrt{M}}\right). \quad (49)$$

□

E Proof of Theorem 3

Proof. For any density matrices $\boldsymbol{\rho}_1, \boldsymbol{\rho}_2 \in \mathbb{X}_r$ in (11), we have

$$\begin{aligned} \|\boldsymbol{\rho}_1 - \boldsymbol{\rho}_2\|_F^2 &= \langle \boldsymbol{\rho}_1 - \boldsymbol{\rho}_2, \boldsymbol{\rho}_1 - \boldsymbol{\rho}_2 \rangle \\ &= \max_{\substack{\boldsymbol{\rho} \in \mathbb{C}^{d^n \times d^n}, \boldsymbol{\rho} = \boldsymbol{\rho}^\dagger, \\ \text{rank}(\boldsymbol{\rho}) = (2r_1, \dots, 2r_{n-1}), \\ \text{trace}(\boldsymbol{\rho}) = 0, \|\boldsymbol{\rho}\|_F \leq \|\boldsymbol{\rho}_1 - \boldsymbol{\rho}_2\|_F}} \langle \boldsymbol{\rho}_1 - \boldsymbol{\rho}_2, \boldsymbol{\rho} \rangle. \end{aligned} \quad (50)$$

Furthermore, we define a restricted Frobenius norm as following:

$$\|\boldsymbol{\rho}_1 - \boldsymbol{\rho}_2\|_{F,2\bar{r}} = \max_{\boldsymbol{\rho} \in \bar{\mathbb{X}}_{2r}} \langle \boldsymbol{\rho}_1 - \boldsymbol{\rho}_2, \boldsymbol{\rho} \rangle. \quad (51)$$

Now, we can expand $\|\boldsymbol{\rho}^{(\tau+1)} - \boldsymbol{\rho}^*\|_F^2$ as following:

$$\begin{aligned} & \|\boldsymbol{\rho}^{(\tau+1)} - \boldsymbol{\rho}^*\|_F^2 = \|\mathcal{P}_{\text{trace}}(\text{SVD}_r^{tt}(\boldsymbol{\rho}^{(\tau)} - \mu \nabla g(\boldsymbol{\rho}^{(\tau)})) - \boldsymbol{\rho}^*)\|_{F,2\bar{r}}^2 \\ & \leq \|\text{SVD}_r^{tt}(\boldsymbol{\rho}^{(\tau)} - \mu \nabla g(\boldsymbol{\rho}^{(\tau)})) - \boldsymbol{\rho}^*\|_{F,2\bar{r}}^2 \\ & \leq \left(1 + \frac{600n}{\underline{\sigma}(\boldsymbol{\rho}^*)}\|\boldsymbol{\rho}^{(0)} - \boldsymbol{\rho}^*\|_F\right) \|\boldsymbol{\rho}^{(\tau)} - \mu \nabla g(\boldsymbol{\rho}^{(\tau)}) - \boldsymbol{\rho}^*\|_{F,2\bar{r}}^2 \\ & = \left(1 + \frac{600n}{\underline{\sigma}(\boldsymbol{\rho}^*)}\|\boldsymbol{\rho}^{(0)} - \boldsymbol{\rho}^*\|_F\right) \left(\|\boldsymbol{\rho}^{(\tau)} - \boldsymbol{\rho}^*\|_F^2 - 2\mu \langle \boldsymbol{\rho}^{(\tau)} - \boldsymbol{\rho}^*, \nabla g(\boldsymbol{\rho}^{(\tau)}) \rangle + \mu^2 \|\nabla g(\boldsymbol{\rho}^{(\tau)})\|_{F,2\bar{r}}^2\right), \end{aligned} \quad (52)$$

where the first and second inequalities follow the nonexpansiveness property of projection onto the convex set and Lemma 4.

First, we need to analyze

$$\begin{aligned} & \langle \boldsymbol{\rho}^{(\tau)} - \boldsymbol{\rho}^*, \nabla g(\boldsymbol{\rho}^{(\tau)}) \rangle \\ & = \sum_{k=1}^K \langle \mathbf{A}_k, \boldsymbol{\rho}^{(\tau)} - \boldsymbol{\rho}^* \rangle^2 - \sum_{k=1}^K \eta_k \langle \mathbf{A}_k, \boldsymbol{\rho}^{(\tau)} - \boldsymbol{\rho}^* \rangle \\ & \geq \frac{d^n(1-\delta)\|\boldsymbol{\rho}^{(\tau)} - \boldsymbol{\rho}^*\|_F^2}{K(d^n+1)} - \frac{c_1 d \bar{r} \sqrt{nd^n(1+\delta)\gamma_t \log n}}{K\sqrt{(d^n+1)M}} \|\boldsymbol{\rho}^{(0)} - \boldsymbol{\rho}^*\|_F, \end{aligned} \quad (53)$$

where the first inequality uses the Lemma 2 and (44) with probability $1 - e^{-c_2 nd^2 \bar{r}^2 \log n}$. Here c_1, c_2 are positive constants.

Then we need to derive

$$\begin{aligned} \|\nabla g(\boldsymbol{\rho}^{(\tau)})\|_{F,2\bar{r}}^2 & \leq 2 \left\| \sum_{k=1}^K \langle \mathbf{A}_k, \boldsymbol{\rho}^{(\tau)} - \boldsymbol{\rho}^* \rangle \mathbf{A}_k \right\|_{F,2\bar{r}}^2 + 2 \left\| \sum_{k=1}^K \eta_k \mathbf{A}_k \right\|_{F,2\bar{r}}^2 \\ & \leq \frac{d^{2n+1}(1+\delta)^2 \|\boldsymbol{\rho}^{(\tau)} - \boldsymbol{\rho}^*\|_F^2}{K^2(d^n+1)^2} + \frac{2c_1^2(1+\delta)\bar{r}^2 nd^{n+2}\gamma_t \log n}{K^2(d^n+1)M}, \end{aligned} \quad (54)$$

where the second inequality respectively follows (44) and

$$\begin{aligned} \left\| \sum_{k=1}^K \langle \mathbf{A}_k, \boldsymbol{\rho}^{(\tau)} - \boldsymbol{\rho}^* \rangle \mathbf{A}_k \right\|_{F,2\bar{r}} & = \max_{\tilde{\boldsymbol{\rho}} \in \bar{\mathbb{X}}_{2r}} \left\langle \sum_{k=1}^K \langle \mathbf{A}_k, \boldsymbol{\rho}^{(\tau)} - \boldsymbol{\rho}^* \rangle \mathbf{A}_k, \tilde{\boldsymbol{\rho}} \right\rangle \\ & = \max_{\tilde{\boldsymbol{\rho}} \in \bar{\mathbb{X}}_{2r}} \sum_{k=1}^K \langle \mathbf{A}_k, \boldsymbol{\rho}^{(\tau)} - \boldsymbol{\rho}^* \rangle \langle \mathbf{A}_k, \tilde{\boldsymbol{\rho}} \rangle \\ & \leq \max_{\tilde{\boldsymbol{\rho}} \in \bar{\mathbb{X}}_{2r}} \frac{d^n(1+\delta)(\langle \boldsymbol{\rho}^{(\tau)} - \boldsymbol{\rho}^*, \tilde{\boldsymbol{\rho}} \rangle + \text{trace}(\boldsymbol{\rho}^{(\tau)} - \boldsymbol{\rho}^*) \text{trace}(\tilde{\boldsymbol{\rho}}))}{K(d^n+1)} \\ & \leq \frac{d^n(1+\delta)\|\boldsymbol{\rho}^{(\tau)} - \boldsymbol{\rho}^*\|_F}{K(d^n+1)}, \end{aligned} \quad (55)$$

where the last line uses Lemma 7.

Combing (53) and (54), we arrive at

$$\begin{aligned}
& \|\boldsymbol{\rho}^{(\tau+1)} - \boldsymbol{\rho}^*\|_F^2 \\
& \leq \left(1 + \frac{600n}{\underline{\sigma}(\boldsymbol{\rho}^*)}\|\boldsymbol{\rho}^{(0)} - \boldsymbol{\rho}^*\|_F\right) \left(\left(1 - \frac{d^{n+1}(1-\delta)\mu}{K(d^n+1)} + \frac{d^{2n+1}(1+\delta)^2\mu^2}{K^2(d^n+1)^2}\right)\|\boldsymbol{\rho}^{(\tau)} - \boldsymbol{\rho}^*\|_F^2 + e\right) \\
& \leq \left(1 + \frac{600n}{\underline{\sigma}(\boldsymbol{\rho}^*)}\|\boldsymbol{\rho}^{(0)} - \boldsymbol{\rho}^*\|_F\right) \left(\left(1 - \frac{d^n(1-\delta)\mu}{K(d^n+1)}\right)\|\boldsymbol{\rho}^{(\tau)} - \boldsymbol{\rho}^*\|_F^2 + e\right) \\
& \leq a^{\tau+1}\|\boldsymbol{\rho}^{(0)} - \boldsymbol{\rho}^*\|_F^2 + \frac{1 + \frac{600n}{\underline{\sigma}(\boldsymbol{\rho}^*)}\|\boldsymbol{\rho}^{(0)} - \boldsymbol{\rho}^*\|_F}{1-a} c_3 \left(\frac{d\bar{r}(1-\delta)\sqrt{n\gamma_t \log n}}{(1+\delta)^{\frac{3}{2}}\sqrt{M}}\|\boldsymbol{\rho}^{(0)} - \boldsymbol{\rho}^*\|_F\right. \\
& \quad \left. + \frac{(1-\delta)^2\bar{r}^2nd^2\gamma_t \log n}{(1+\delta)^3M}\right) \\
& \leq a^{\tau+1}\|\boldsymbol{\rho}^{(0)} - \boldsymbol{\rho}^*\|_F^2 + c_4 \left(\frac{d\bar{r}(1-\delta)\sqrt{n\gamma_t \log n}}{(1+\delta)^{\frac{3}{2}}\sqrt{M}}\|\boldsymbol{\rho}^{(0)} - \boldsymbol{\rho}^*\|_F + \frac{(1-\delta)^2\bar{r}^2nd^2\gamma_t \log n}{(1+\delta)^3M}\right), \tag{56}
\end{aligned}$$

where we define the error term $e = \frac{2\mu c_1 d\bar{r}\sqrt{nd^n(1+\delta)\gamma_t \log n}}{K\sqrt{(d^n+1)M}}\|\boldsymbol{\rho}^{(0)} - \boldsymbol{\rho}^*\|_F + \frac{2\mu^2 c_1^2(1+\delta)\bar{r}^2nd^{n+2}\gamma_t \log n}{K^2(d^n+1)M}$, and c_3, c_4 are positive constants.

The last two lines follow assumptions with regard to the step size and initialization: $\frac{\frac{600n}{\underline{\sigma}(\boldsymbol{\rho}^*)}\|\boldsymbol{\rho}^{(0)} - \boldsymbol{\rho}^*\|_F}{1 + \frac{600n}{\underline{\sigma}(\boldsymbol{\rho}^*)}\|\boldsymbol{\rho}^{(0)} - \boldsymbol{\rho}^*\|_F} \frac{K(d^n+1)}{d^n(1-\delta)} < \mu \leq \frac{(d-1)(d^n+1)(1-\delta)K}{(1+\delta)^2d^{n+1}}$ and $\|\boldsymbol{\rho}^{(0)} - \boldsymbol{\rho}^*\|_F < \frac{\underline{\sigma}(\boldsymbol{\rho}^*)(d-1)(1-\delta)^2}{600n(1+\delta^2+(4d-2)\delta)}$ which guarantee that the convergence rate satisfies

$$a = \left(1 + \frac{600n}{\underline{\sigma}(\boldsymbol{\rho}^*)}\|\boldsymbol{\rho}^{(0)} - \boldsymbol{\rho}^*\|_F\right) \left(1 - \frac{d^n(1-\delta)\mu}{K(d^n+1)}\right) < 1. \tag{57}$$

□

F Proof of Theorem 4

Proof. By the definition of the restricted Frobenius norm (51), we can analyze

$$\begin{aligned}
\|\boldsymbol{\rho}^{(0)} - \boldsymbol{\rho}^*\|_F & = \left\| \mathcal{P}_{\text{trace}} \left(\text{SVD}_{\mathbf{r}}^{tt} \left(\sum_{k=1}^K \frac{K(d^n+1)}{d^n} (\langle \mathbf{A}_k, \boldsymbol{\rho}^* \rangle + \eta_k) \mathbf{A}_k \right) - \boldsymbol{\rho}^* \right) \right\|_{F, 2\bar{r}} \\
& \leq \left\| \text{SVD}_{\mathbf{r}}^{tt} \left(\sum_{k=1}^K \frac{K(d^n+1)}{d^n} (\langle \mathbf{A}_k, \boldsymbol{\rho}^* \rangle + \eta_k) \mathbf{A}_k \right) - \boldsymbol{\rho}^* \right\|_{F, 2\bar{r}} \\
& \leq (1 + \sqrt{n-1}) \left\| \sum_{k=1}^K \frac{K(d^n+1)}{d^n} (\langle \mathbf{A}_k, \boldsymbol{\rho}^* \rangle + \eta_k) \mathbf{A}_k - \boldsymbol{\rho}^* \right\|_{F, 2\bar{r}} \\
& \leq (1 + \sqrt{n-1}) \left(\frac{K(d^n+1)}{d^n} \left\| \sum_{k=1}^K \eta_k \mathbf{A}_k \right\|_{F, 2\bar{r}} + \left\| \sum_{k=1}^K \frac{K(d^n+1)}{d^n} \langle \mathbf{A}_k, \boldsymbol{\rho}^* \rangle \mathbf{A}_k - \boldsymbol{\rho}^* \right\|_{F, 2\bar{r}} \right) \\
& \leq (1 + \sqrt{n-1}) \left(\frac{c_1 d\bar{r} \sqrt{(1+\delta)(d^n+1)n\gamma_t \log n}}{\sqrt{d^n M}} + \delta \|\boldsymbol{\rho}^*\|_F \right), \tag{58}
\end{aligned}$$

where the first two inequalities respectively follows the nonexpansiveness property of the projection onto the convex set and the quasi-optimality property of TT-SVD projection [27]. In the last line, the upper bound of $\left\| \sum_{k=1}^K \eta_k \mathbf{A}_k \right\|_{F, 2\bar{r}}$ can be directly obtained from (41) with probability $1 - e^{-c_2nd^2\bar{r}^2 \log n}$ with constants $c_i, i = 1, 2$. Additionally, based

on Lemma 7, we have

$$\begin{aligned}
& \left\| \sum_{k=1}^K \frac{K(d^n + 1)}{d^n} \langle \mathbf{A}_k, \boldsymbol{\rho}^* \rangle \mathbf{A}_k - \boldsymbol{\rho}^* \right\|_{F, 2\bar{r}} \\
&= \max_{\tilde{\boldsymbol{\rho}} \in \bar{\mathbb{X}}_{2r}} \left\langle \sum_{k=1}^K \frac{K(d^n + 1)}{d^n} \langle \mathbf{A}_k, \boldsymbol{\rho}^* \rangle \mathbf{A}_k - \boldsymbol{\rho}^*, \tilde{\boldsymbol{\rho}} \right\rangle \\
&= \max_{\tilde{\boldsymbol{\rho}} \in \bar{\mathbb{X}}_{2r}} (1 + \delta) (\langle \boldsymbol{\rho}^*, \tilde{\boldsymbol{\rho}} \rangle + \text{trace}(\boldsymbol{\rho}^*) \text{trace}(\tilde{\boldsymbol{\rho}})) - \langle \boldsymbol{\rho}^*, \tilde{\boldsymbol{\rho}} \rangle \leq \delta \|\boldsymbol{\rho}^*\|_F.
\end{aligned} \tag{59}$$

□

G Auxiliary Materials

Lemma 5. ([39, Lemma 3]) *The integral over the Haar measure in (5) is given by*

$$\int (\mathbf{w}\mathbf{w}^\dagger)^{\otimes s} d\mathbf{w} = \frac{1}{C_{d^n+s-1}^s} P_{\text{Sym}}, \tag{60}$$

where P_{Sym} is the projector over the symmetric subspace.

Lemma 6. ([1, Lemma 10]) *For any $\mathbf{A}_i, \mathbf{A}_i^* \in \mathbb{R}^{r_{i-1} \times r_i}$, $i = 1, \dots, N$, we have*

$$\mathbf{A}_1 \mathbf{A}_2 \cdots \mathbf{A}_N - \mathbf{A}_1^* \mathbf{A}_2^* \cdots \mathbf{A}_N^* = \sum_{i=1}^N \mathbf{A}_1^* \cdots \mathbf{A}_{i-1}^* (\mathbf{A}_i - \mathbf{A}_i^*) \mathbf{A}_{i+1} \cdots \mathbf{A}_N. \tag{61}$$

Lemma 7. *For arbitrary Hermitian matrix $\boldsymbol{\rho}_1, \boldsymbol{\rho}_2 \in \mathbb{C}^{d^n \times d^n}$ and a set of δ -approximate 2-design POVMs $\mathbf{A}_k = \frac{d^n}{K} \mathbf{w}_k \mathbf{w}_k^\dagger$, $k \in [K]$ in Definition 3, we have*

$$\sum_{k=1}^K \langle \mathbf{A}_k, \boldsymbol{\rho}_1 \rangle \langle \mathbf{A}_k, \boldsymbol{\rho}_2 \rangle \leq (1 + \delta) \frac{d^n (\text{trace}(\boldsymbol{\rho}_1) \text{trace}(\boldsymbol{\rho}_2) + \text{trace}(\boldsymbol{\rho}_1 \boldsymbol{\rho}_2))}{K(d^n + 1)}. \tag{62}$$

Proof.

$$\begin{aligned}
\sum_{k=1}^K \langle \mathbf{A}_k, \boldsymbol{\rho}_1 \rangle \langle \mathbf{A}_k, \boldsymbol{\rho}_2 \rangle &= \sum_{k=1}^K \text{trace}((\mathbf{A}_k \boldsymbol{\rho}_1) \otimes (\mathbf{A}_k \boldsymbol{\rho}_2)) \\
&= \sum_{k=1}^K \text{trace}(\mathbf{A}_k^{\otimes 2} (\boldsymbol{\rho}_1 \otimes \boldsymbol{\rho}_2)) \\
&\leq (1 + \delta) \frac{d^n \text{trace}((\mathbf{I} + \mathbf{S})(\boldsymbol{\rho}_1 \otimes \boldsymbol{\rho}_2))}{K(d^n + 1)} \\
&= (1 + \delta) \frac{d^n (\text{trace}(\boldsymbol{\rho}_1) \text{trace}(\boldsymbol{\rho}_2) + \text{trace}(\boldsymbol{\rho}_1 \boldsymbol{\rho}_2))}{K(d^n + 1)},
\end{aligned} \tag{63}$$

where the penultimate line follows (6) and (35), and the last line is from [16, Lemma 17]. □

References

- [1] Zhen Qin, Casey Jameson, Zhexuan Gong, Michael B Wakin, and Zhihui Zhu. Quantum state tomography for matrix product density operators. *IEEE Transactions on Information Theory*, 70(7):5030–5056, 2024.
- [2] Michael A Nielsen and Isaac Chuang. Quantum computation and quantum information, 2002.

- [3] K Vogel and H Risken. Determination of quasiprobability distributions in terms of probability distributions for the rotated quadrature phase. *Physical Review A*, 40(5):2847, 1989.
- [4] Zdenek Hradil. Quantum-state estimation. *Physical Review A*, 55(3):R1561, 1997.
- [5] J Řeháček, Z Hradil, and M Ježek. Iterative algorithm for reconstruction of entangled states. *Physical Review A*, 63(4):040303, 2001.
- [6] Robin Blume-Kohout. Optimal, reliable estimation of quantum states. *New Journal of Physics*, 12(4):043034, 2010.
- [7] Christopher Granade, Joshua Combes, and DG Cory. Practical bayesian tomography. *new Journal of Physics*, 18(3):033024, 2016.
- [8] Joseph M Lukens, Kody JH Law, Ajay Jasra, and Pavel Lougovski. A practical and efficient approach for bayesian quantum state estimation. *New Journal of Physics*, 22(6):063038, 2020.
- [9] Robin Blume-Kohout. Robust error bars for quantum tomography. *arXiv:1202.5270*, 2012.
- [10] Philippe Faist and Renato Renner. Practical and reliable error bars in quantum tomography. *Physical review letters*, 117(1):010404, 2016.
- [11] Anastasios Kyriillidis, Amir Kalev, Dohyung Park, Srinadh Bhojanapalli, Constantine Caramanis, and Sujay Sanghavi. Provable compressed sensing quantum state tomography via non-convex methods. *npj Quantum Information*, 4(1):1–7, 2018.
- [12] Fernando GSL Brandão, Richard Kueng, and Daniel Stilck França. Fast and robust quantum state tomography from few basis measurements. *arXiv:2009.08216*, 2020.
- [13] Giacomo Torlai, Guglielmo Mazzola, Juan Carrasquilla, Matthias Troyer, Roger Melko, and Giuseppe Carleo. Neural-network quantum state tomography. *Nature Physics*, 14(5):447–450, 2018.
- [14] Giuseppe Carleo, Ignacio Cirac, Kyle Cranmer, Laurent Daudet, Maria Schuld, Naftali Tishby, Leslie Vogt-Maranto, and Lenka Zdeborová. Machine learning and the physical sciences. *Reviews of Modern Physics*, 91(4):045002, 2019.
- [15] Sanjaya Lohani, Brian T Kirby, Michael Brodsky, Onur Danaci, and Ryan T Glasser. Machine learning assisted quantum state estimation. *Machine Learning: Science and Technology*, 1(3):035007, 2020.
- [16] Richard Kueng, Holger Rauhut, and Ulrich Terstiege. Low rank matrix recovery from rank one measurements. *Applied and Computational Harmonic Analysis*, 42(1):88–116, 2017.
- [17] Madalin Guță, Jonas Kahn, Richard Kueng, and Joel A Tropp. Fast state tomography with optimal error bounds. *Journal of Physics A: Mathematical and Theoretical*, 53(20):204001, 2020.
- [18] Daniel Stilck França, Fernando GS Brandão, and Richard Kueng. Fast and robust quantum state tomography from few basis measurements. In *16th Conference on the Theory of Quantum Computation, Communication and Cryptography (TQC 2021)*. Schloss Dagstuhl-Leibniz-Zentrum für Informatik, 2021.
- [19] Yi-Kai Liu. Universal low-rank matrix recovery from pauli measurements. *Advances in Neural Information Processing Systems*, 24, 2011.
- [20] J Haah, AW Harrow, Z Ji, X Wu, and N Yu. Sample-optimal tomography of quantum states. *IEEE Transactions on Information Theory*, 63(9):5628–5641, 2017.
- [21] Vladislav Voroninski. Quantum tomography from few full-rank observables. *arXiv:1309.7669*, 2013.
- [22] John Preskill. Quantum computing in the nisq era and beyond. *Quantum*, 2:79, 2018.

- [23] Frank Arute, Kunal Arya, Ryan Babbush, Dave Bacon, Joseph C Bardin, Rami Barends, Rupak Biswas, Sergio Boixo, Fernando GSL Brandao, David A Buell, et al. Quantum supremacy using a programmable superconducting processor. *Nature*, 574(7779):505–510, 2019.
- [24] Jerry Chow, Oliver Dial, and Jay Gambetta. Ibm quantum breaks the 100-qubit processor barrier. *IBM Research Blog*, 2021.
- [25] Albert H Werner, Daniel Jaschke, Pietro Silvi, Martin Kliesch, Tommaso Calarco, Jens Eisert, and Simone Montangero. Positive tensor network approach for simulating open quantum many-body systems. *Physical review letters*, 116(23):237201, 2016.
- [26] Kyungjoo Noh, Liang Jiang, and Bill Fefferman. Efficient classical simulation of noisy random quantum circuits in one dimension. *Quantum*, 4:318, 2020.
- [27] Ivan V Oseledets. Tensor-train decomposition. *SIAM Journal on Scientific Computing*, 33(5):2295–2317, 2011.
- [28] J. Eisert, M. Cramer, and M. B. Plenio. Colloquium: Area laws for the entanglement entropy. *Rev. Mod. Phys.*, 82:277–306, Feb 2010.
- [29] Bogdan Pirvu, Valentin Murg, J Ignacio Cirac, and Frank Verstraete. Matrix product operator representations. *New Journal of Physics*, 12(2):025012, 2010.
- [30] Tillmann Baumgratz, David Gross, Marcus Cramer, and Martin B Plenio. Scalable reconstruction of density matrices. *Physical review letters*, 111(2):020401, 2013.
- [31] Mahn-Soo Choi. Single-qubit reaped quantum state tomography. *Scientific reports*, 12(1):10983, 2022.
- [32] Alexander Lidiak, Casey Jameson, Zhen Qin, Gongguo Tang, Michael B Wakin, Zhihui Zhu, and Zhexuan Gong. Quantum state tomography with tensor train cross approximation. *arXiv:2207.06397*, 2022.
- [33] Joseph M Renes. Equiangular spherical codes in quantum cryptography. *arXiv preprint quant-ph/0409043*, 2004.
- [34] AJ Scott, Jonathan Walgate, and Barry C Sanders. Optimal fingerprinting strategies with one-sided error. *arXiv preprint quant-ph/0507048*, 2005.
- [35] Carlton M Caves, Christopher A Fuchs, and Rüdiger Schack. Unknown quantum states: the quantum de finetti representation. *Journal of Mathematical Physics*, 43(9):4537–4559, 2002.
- [36] Robert König and Renato Renner. A de finetti representation for finite symmetric quantum states. *Journal of Mathematical physics*, 46(12), 2005.
- [37] Joseph M Renes, Robin Blume-Kohout, Andrew J Scott, and Carlton M Caves. Symmetric informationally complete quantum measurements. *Journal of Mathematical Physics*, 45(6):2171–2180, 2004.
- [38] Gerhard Zauner. *Quantum Designs*. PhD thesis, Ph. D. thesis, University of Vienna Vienna, 1999.
- [39] Michele Dall’Arno. Accessible information and informational power of quantum 2-designs. *Physical Review A*, 90(5):052311, 2014.
- [40] Christopher J Hillar and Lek-Heng Lim. Most tensor problems are np-hard. *Journal of the ACM (JACM)*, 60(6):1–39, 2013.
- [41] E Prugovečki. Information-theoretical aspects of quantum measurement. *International Journal of Theoretical Physics*, 16(5):321–331, 1977.
- [42] Paul Busch and Pekka J Lahti. The determination of the past and the future of a physical system in quantum mechanics. *Foundations of Physics*, 19:633–678, 1989.
- [43] Asher Peres. *Quantum theory: concepts and methods*, volume 72. Springer, 1997.

- [44] Stefan Weigert. Simple minimal informationally complete measurements for qudits. *International Journal of Modern Physics B*, 20(11n13):1942–1955, 2006.
- [45] Steven T Flammia. On sic-povms in prime dimensions. *Journal of Physics A: Mathematical and General*, 39(43):13483, 2006.
- [46] Isabelle Jianing Geng, Kimberly Golubeva, and Gilad Gour. What are the minimal conditions required to define a sic povm? *arXiv preprint arXiv:2007.10483*, 2020.
- [47] Gary Greaves, Jacobus H Koolen, Akihiro Munemasa, and Ferenc Szöllősi. Equiangular lines in euclidean spaces. *Journal of Combinatorial Theory, Series A*, 138:208–235, 2016.
- [48] Mátyás A Sustik, Joel A Tropp, Inderjit S Dhillon, and Robert W Heath Jr. On the existence of equiangular tight frames. *Linear Algebra and its applications*, 426(2-3):619–635, 2007.
- [49] Andrew J Scott. Tight informationally complete quantum measurements. *Journal of Physics A: Mathematical and General*, 39(43):13507, 2006.
- [50] Thomas Durt, Christian Kurtsiefer, Antia Lamas-Linares, and Alexander Ling. Wigner tomography of two-qubit states and quantum cryptography. *Physical Review A—Atomic, Molecular, and Optical Physics*, 78(4):042338, 2008.
- [51] Andrew James Scott and Markus Grassl. Symmetric informationally complete positive-operator-valued measures: A new computer study. *Journal of Mathematical Physics*, 51(4), 2010.
- [52] SB Samuel and Z Gedik. Sic-povms and the knaster’s conjecture. *arXiv preprint arXiv:2405.16733*, 2024.
- [53] Ingemar Bengtsson, Markus Grassl, and Gary McConnell. Sic-povms from stark units: Dimensions $n^2 + 3 = 4p$, p prime. *arXiv preprint arXiv:2403.02872*, 2024.
- [54] David L Donoho. Compressed sensing. *IEEE Transactions on information theory*, 52(4):1289–1306, 2006.
- [55] Emmanuel J Candès, Justin Romberg, and Terence Tao. Robust uncertainty principles: Exact signal reconstruction from highly incomplete frequency information. *IEEE Transactions on information theory*, 52(2):489–509, 2006.
- [56] Emmanuel J Candès and Michael B Wakin. An introduction to compressive sampling. *IEEE signal processing magazine*, 25(2):21–30, 2008.
- [57] Benjamin Recht, Maryam Fazel, and Pablo A Parrilo. Guaranteed minimum-rank solutions of linear matrix equations via nuclear norm minimization. *SIAM review*, 52(3):471–501, 2010.
- [58] Armin Eftekhari and Michael B Wakin. New analysis of manifold embeddings and signal recovery from compressive measurements. *Applied and Computational Harmonic Analysis*, 39(1):67–109, 2015.
- [59] William Matthews, Stephanie Wehner, and Andreas Winter. Distinguishability of quantum states under restricted families of measurements with an application to quantum data hiding. *Communications in Mathematical Physics*, 291:813–843, 2009.
- [60] David Gross, Felix Kraemer, and Richard Kueng. A partial derandomization of phaselift using spherical designs. *Journal of Fourier Analysis and Applications*, 21(2):229–266, 2015.
- [61] Paul D Seymour and Thomas Zaslavsky. Averaging sets: a generalization of mean values and spherical designs. *Advances in Mathematics*, 52(3):213–240, 1984.
- [62] Bela Bajnok. Construction of spherical t-designs. *Geometriae Dedicata*, 43:167–179, 1992.
- [63] A Hayashi, T Hashimoto, and M Horibe. Reexamination of optimal quantum state estimation of pure states. *Physical Review A—Atomic, Molecular, and Optical Physics*, 72(3):032325, 2005.

- [64] Andris Ambainis and Joseph Emerson. Quantum t-designs: t-wise independence in the quantum world. In *Twenty-Second Annual IEEE Conference on Computational Complexity (CCC'07)*, pages 129–140. IEEE, 2007.
- [65] Frank Verstraete, Juan J Garcia-Ripoll, and Juan Ignacio Cirac. Matrix product density operators: Simulation of finite-temperature and dissipative systems. *Physical review letters*, 93(20):207204, 2004.
- [66] Krzysztof Zajkowski. Bounds on tail probabilities for quadratic forms in dependent sub-gaussian random variables. *Statistics & Probability Letters*, 167:108898, 2020.
- [67] Roman Vershynin. *High-dimensional probability: An introduction with applications in data science*, volume 47. Cambridge university press, 2018.
- [68] Zak Webb. The clifford group forms a unitary 3-design. *arXiv preprint arXiv:1510.02769*, 2015.
- [69] Huangjun Zhu. Multiqubit clifford groups are unitary 3-designs. *Physical Review A*, 96(6):062336, 2017.
- [70] Jonas Helsen, Joel J Wallman, and Stephanie Wehner. Representations of the multi-qubit clifford group. *Journal of Mathematical Physics*, 59(7), 2018.
- [71] Andreas Ketterer, Nikolai Wyderka, and Otfried Gühne. Entanglement characterization using quantum designs. *Quantum*, 4:325, 2020.
- [72] Patrick J Coles, M Cerezo, and Lukasz Cincio. Strong bound between trace distance and hilbert-schmidt distance for low-rank states. *Physical Review A*, 100(2):022103, 2019.
- [73] Laurent Condat. Fast projection onto the simplex and the l_1 ball. *Mathematical Programming*, 158(1-2):575–585, 2016.
- [74] Holger Rauhut, Reinhold Schneider, and Željka Stojanac. Low rank tensor recovery via iterative hard thresholding. *Linear Algebra and its Applications*, 523:220–262, 2017.
- [75] Holger Rauhut, Reinhold Schneider, and Željka Stojanac. Tensor completion in hierarchical tensor representations. In *Compressed sensing and its applications*, pages 419–450. Springer, 2015.
- [76] Stanislav Budzinskiy and Nikolai Zamarashkin. Tensor train completion: local recovery guarantees via riemannian optimization. *arXiv:2110.03975*, 2021.
- [77] Zhen Qin, Michael B Wakin, and Zhihui Zhu. Guaranteed nonconvex factorization approach for tensor train recovery. *arXiv preprint arXiv:2401.02592*, 2024.
- [78] Zhen Qin and Zhihui Zhu. Computational and statistical guarantees for tensor-on-tensor regression with tensor train decomposition. *arXiv preprint arXiv:2406.06002*, 2024.
- [79] Xian-Da Zhang. *Matrix analysis and applications*. Cambridge University Press, 2017.
- [80] Jian-Feng Cai, Jingyang Li, and Dong Xia. Provable tensor-train format tensor completion by riemannian optimization. *Journal of Machine Learning Research*, 23(123):1–77, 2022.
- [81] Yue M Lu and Gen Li. Phase transitions of spectral initialization for high-dimensional non-convex estimation. *Information and Inference: A Journal of the IMA*, 9(3):507–541, 2020.
- [82] Emmanuel J Candès, Xiaodong Li, and Mahdi Soltanolkotabi. Phase retrieval via wirtinger flow: Theory and algorithms. *IEEE Transactions on Information Theory*, 61(4):1985–2007, 2015.
- [83] Wangyu Luo, Wael Alghamdi, and Yue M Lu. Optimal spectral initialization for signal recovery with applications to phase retrieval. *IEEE Transactions on Signal Processing*, 67(9):2347–2356, 2019.
- [84] Cong Ma, Yuanxin Li, and Yuejie Chi. Beyond procrustes: Balancing-free gradient descent for asymmetric low-rank matrix sensing. *IEEE Transactions on Signal Processing*, 69:867–877, 2021.

- [85] Tian Tong, Cong Ma, and Yuejie Chi. Accelerating ill-conditioned low-rank matrix estimation via scaled gradient descent. *J. Mach. Learn. Res.*, 22:150–1, 2021.
- [86] R. Han, R. Willett, and A. R. Zhang. An optimal statistical and computational framework for generalized tensor estimation. *arXiv:2002.11255*, 2020.
- [87] Tian Tong, Cong Ma, Ashley Prater-Bennette, Erin Tripp, and Yuejie Chi. Scaling and scalability: Provable nonconvex low-rank tensor estimation from incomplete measurements. *arXiv:2104.14526*, Nov. 2021.
- [88] Léon Bottou, Frank E Curtis, and Jorge Nocedal. Optimization methods for large-scale machine learning. *SIAM review*, 60(2):223–311, 2018.
- [89] Roman Stricker, Michael Meth, Lukas Postler, Claire Edmunds, Chris Ferrie, Rainer Blatt, Philipp Schindler, Thomas Monz, Richard Kueng, and Martin Ringbauer. Experimental single-setting quantum state tomography. *PRX Quantum*, 3(4):040310, 2022.
- [90] Casey Jameson, Zhen Qin, Alireza Goldar, Michael B. Wakin, Zihui Zhu, and Zhexuan Gong. Optimal quantum state tomography with local informationally complete measurements. *arXiv:2408.07115*, 2024.
- [91] Alexey E Rastegin. Notes on general sic-povms. *Physica Scripta*, 89(8):085101, 2014.
- [92] Gilad Gour and Amir Kalev. Construction of all general symmetric informationally complete measurements. *Journal of Physics A: Mathematical and Theoretical*, 47(33):335302, 2014.
- [93] Antonio Anna Mele. Introduction to haar measure tools in quantum information: A beginner’s tutorial. *arXiv preprint arXiv:2307.08956*, 2023.
- [94] Hsin-Yuan Huang, Richard Kueng, and John Preskill. Predicting many properties of a quantum system from very few measurements. *Nature Physics*, 16(10):1050–1057, 2020.
- [95] ID Coope. On matrix trace inequalities and related topics for products of hermitian matrices. *Journal of mathematical analysis and applications*, 188(3):999–1001, 1994.